

Hadronic Parity Violation: a New View through the Looking Glass

Michael J. Ramsey-Musolf
Kellogg Radiation Laboratory,
California Institute of Technology,
Pasadena, CA 91125 USA

and

Shelley A. Page
Dept. of Physics & Astronomy,
Univ. of Manitoba,
Winnipeg, MB R3T 2N2 Canada

October 16, 2018

Abstract

Studies of the strangeness changing hadronic weak interaction have produced a number of puzzles that have so far evaded a complete explanation within the Standard Model. Their origin may lie either in dynamics peculiar to weak interactions involving strange quarks or in more general aspects of the interplay between strong and weak interactions. In principle, studies of the strangeness conserving hadronic weak interaction using parity violating hadronic and nuclear observables provide a complementary window on this question. However, progress in this direction has been hampered by the lack of a suitable theoretical framework for interpreting hadronic parity violation measurements in a model-independent way. Recent work involving effective field theory ideas has led to the formulation of such a framework while motivating the development of a number of new hadronic parity violation experiments in few-body systems. In this article, we review these recent developments and discuss the prospects and opportunities for further experimental and theoretical progress.

Contents

1	Introduction	3
2	Weak Meson Exchange Model Meets the End of the Road	7
2.1	Meson Exchange Model of the Weak N-N Interaction	8
2.2	Experimental Progress	12
2.2.1	Longitudinal Analyzing Power in pp Scattering	13
2.2.2	Progress in the np System	18
2.2.3	Neutron Spin Rotation Experiments	21
2.2.4	Nuclear Anapole Moments	23
2.2.5	Parity Violation in Compound Nuclei	25
2.3	The End of the Road	26
3	Effective Field Theory Framework	27
3.1	The Pionless Effective Field Theory	28
3.2	PV EFT with Pions	34
3.3	Recent Theoretical Work	40
3.4	Experimental Prospects	45
4	Beyond Hadronic Parity Violation	47
5	Summary and Conclusions	49
6	Acknowledgements	50

1 Introduction

Explaining the weak interactions of quarks in terms of the dynamics of the Standard Model (SM) has been an area of vigorous research in nuclear and particle physics for several decades. Experimentally, the hadronic weak interaction (HWI) is probed by observing non-leptonic, flavor changing decays of mesons and baryons and by measuring observables that conserve flavor but violate the parity symmetry of the strong and electromagnetic interactions. Theoretically, the problem has been a particularly challenging one, requiring the computation of low-energy weak matrix elements of the HWI in strongly interacting systems. Although the structure of the weak quark-quark interaction in the SM has been well established for some time, its manifestation in strongly interacting systems remains only partially understood. The stumbling block has been the non-perturbative nature of quantum chromodynamics (QCD) at low energies. In contending with it, theorists have resorted to a variety of approximation schemes to obtain physically reasonable estimates of HWI observables. Ultimately, however, arriving at definitive, SM predictions requires that one treat the non-perturbative QCD dynamics in a rigorous way.

In the case of the flavor changing decays of mesons, use of effective field theory (EFT) techniques – chiral perturbation theory (χ PT), heavy quark effective theory (HQET), and recently, soft collinear effective theory (SCET) – have led to enormous progress. In each instance, the presence of distinct physical scales at play in the processes of interest allows one to carry out a systematic expansion of the effective Lagrangian in powers of scale ratios while incorporating the symmetries of QCD into the structure of the operators. The operator coefficients that encode the non-perturbative QCD dynamics are obtained from measurement, and the structure of the EFT is then used to translate this information into predictions for other observables. Moreover, a meaningful confrontation of experiment with QCD theory can be made, as computations of the operator coefficients can in principle be performed on the lattice.

The situation involving the HWI of baryons is far less satisfactory, and decades of experimental and theoretical work have left us with a number of unresolved puzzles. In the case of hyperon non-leptonic decays, for example, one has not yet been able to find a simultaneous accounting of both the parity conserving P-wave and parity violating (PV) S-wave decay amplitudes. Similarly, the PV asymmetries associated with the radiative decays of hyperons are anomalously large. In the limit of degenerate u-, d-, and s-quarks, SU(3) flavor symmetry implies that these asymmetries must vanish. Given the known mass splitting between the strange and two light flavors, one would expect the asymmetries to have magnitudes of order $m_s/M_B \sim 0.15$, where $M_B \sim 1$ GeV is a typical hyperon mass. The experimental asymmetries, in contrast, are four-to-five times larger in magnitude. Even the well-known $\Delta I = 1/2$ rule that summarizes the observed dominance of the $I = 1/2$ channel over the $I = 3/2$ channel in strangeness changing nonleptonic decays remains enigmatic, as no apparent symmetry favors either channel. In short, consideration of QCD symmetries and the relevant physical scales does not suffice to account for the observed properties of the $\Delta S = 1$ HWI.

While the puzzles surrounding the strangeness changing HWI have been discussed extensively elsewhere, the $\Delta S = 0$ HWI has generally received less attention. Nonethe-

less, since we do not know whether the breakdown of QCD symmetry-based expectations in the $\Delta S = 1$ sector results from the presence of a dynamical strange quark or from other, yet-to-be-uncovered dynamics, consideration of the $\Delta S = 0$ HWI – for which the strange quark plays a relatively minor role – is no less important. In the following review, we focus on this component of the HWI.

According to the SM, the structure of the low-energy $\Delta S = 0$ HWI is relatively simple:

$$\mathcal{H}_{\text{HWI}}^{\Delta S=0} = \frac{G_F}{\sqrt{2}} \left(J_\lambda^{CC\dagger} J^{\lambda CC} + \frac{1}{2} J_\lambda^{NC\dagger} J^{\lambda NC} \right) \quad (1)$$

where G_F is the Fermi constant and where J_λ^{CC} and J_λ^{NC} are the weak charged and neutral currents, respectively. The theoretical challenge is to find the appropriate effective interaction $\mathcal{H}_{\text{HWI}}^{\Delta S=0 \text{ eff}}(N, \pi, \Delta, \dots)$ that best describes the hadronic manifestation of $\mathcal{H}_{\text{HWI}}^{\Delta S=0}$. Because J_λ^{CC} transforms as a doublet under strong isospin while J_λ^{NC} contains $I = 0$ and $I = 1$ components, the current-current products in $\mathcal{H}_{\text{HWI}}^{\Delta S=0}$ contain terms that transform as isoscalars, isovectors, and isotensors. Consequently, $\mathcal{H}_{\text{HWI}}^{\Delta S=0 \text{ eff}}$ must contain the most general set of operators having the same isospin properties. In what follows, we review the theoretical efforts to determine this effective interaction.

Experimentally, the $\Delta S = 0$ HWI can be isolated solely via hadronic and nuclear physics processes that violate parity, thereby filtering out the much larger effects of the strangeness conserving strong and electromagnetic interactions. Efforts to do so are not new. Soon after the 1957 discovery of parity violation in μ -decay and nuclear β -decay, the search was on for evidence of a PV weak nuclear force that would result in small, parity violating effects in nuclear observables. That year, Tanner reported the first experimental search for a PV nucleon-nucleon (NN) interaction (1). Subsequently, Feynman and Gell-Mann (2) predicted that the four fermion interactions responsible for leptonic and semi-leptonic weak decays should have a four nucleon partner that is similarly first order in G_F . A decade later, Lobashov et al. produced the first definitive evidence for the existence of a first order weak NN force in radiative neutron capture on ^{181}Ta that was consistent with the Feynman and Gell-Mann hypothesis (3, 4).

The pursuit of this evidence in the Tanner, Lobashov and subsequent experiments was challenging, as one expected the magnitude of the PV effects to be $\mathcal{O}(10^{-7})$. Along the way, it was realized that certain accidents of nuclear structure in many-body nuclei could amplify the expected PV effects by several orders of magnitude, and a $\sim 10\%$ PV effect was, indeed, observed in ^{139}La (5). The amplification arises from two sources: the presence of nearly degenerate opposite parity states that are mixed by the HWI, and the interference of an otherwise parity forbidden transition amplitude with a much larger parity allowed one. Subsequent experiments then yielded a mix of PV measurements in nuclei, where one expected amplification factors of order 10^2 to 10^3 , as well studies of PV observables in the scattering of polarized protons and neutrons from hadronic targets.

Theoretically, however, the use of nuclear systems introduces an additional level of complication in the interpretation of experiments, as one must contend with both nuclear structure effects as well as the dynamics of non-perturbative QCD. For over two decades now, the conventional framework for carrying out this interpretation has been a meson exchange model, popularized by the seminal work of Desplanques, Donoghue, and

Holstein (DDH) (6). The model assumes that the PV nucleon-nucleon (NN) interaction is dominated by the exchange of the pion and two lightest vector mesons (ρ and ω), and its strength is characterized by seven PV meson-nucleon couplings: h_π^1 , $h_\rho^{0,1,2}$, $h_\rho^{1'}$ and $h_\omega^{0,1}$, where the superscript indicates the isospin¹. DDH provided theoretical “reasonable ranges” and “best values” for the h_M^i using SU(6) symmetry, constraints from non-leptonic hyperon decay data, and the quark model to estimate the experimentally unconstrained terms. Despite various attempts to improve upon the original DDH work, the results of their analysis still remain as the benchmark, theoretical targets for the PV meson-nucleon couplings.

The experimental results from nuclear and hadronic PV measurements have been analyzed using the DDH framework, leading to constraints on combinations of the h_M^i that typically enter PV observables. The results are in general agreement with the DDH reasonable ranges, though the ranges themselves are quite broad, and the constraints from different experiments are not entirely consistent with each other. A particular quandary involves h_π^1 : the γ -decays of ^{18}F imply that it is consistent with zero, while the analysis of the ^{133}Cs anapole moment differs from zero by several standard deviations (7). More to the point, the connection between the PV experiments and SM expectations is far from transparent. Indeed, in order to draw this connection using the meson-exchange framework and nuclear PV observables, one has to sort through a number of model dependent effects involving nuclear structure, hadron structure, and the meson exchange model itself. Whether one has a reasonable hope for doing so in a systematic manner is debatable at best.

At the end of the day, the goal of studying the $\Delta S = 0$ HWI with hadronic and nuclear PV is to help determine the degree to which the symmetries of QCD characterize the realization of the HWI in strongly interacting systems and, as a corollary, to shed light on the long standing puzzles in the $\Delta S = 1$ sector. To that end, one would ideally formulate the problem to make the contact with the underlying SM as transparent as possible while avoiding hadronic model and nuclear structure ambiguities. Recently, a framework for doing so has been formulated in Reference (8) using effective field theory ideas. That work builds on the extensive developments in the past decade of an EFT for the strong NN interaction that has been applied successfully to a variety of few-body nuclear phenomena. In the case of the PV NN force, two versions of the EFT are useful, depending on the energy scales present in the process under consideration:

- (I) For energies well below the pion mass, the EFT contains only four-nucleon operators and five effective parameters, or “low-energy constants”, that characterize the five independent low-energy S-wave/P-wave mixing matrix elements: $\lambda_s^{0,1,2}$, λ_t , and ρ_t . Relative to the leading order parity-conserving four nucleon operators, the PV operators are $\mathcal{O}(Q)$, where Q is a small energy scale. In this version of the EFT, the pion is considered to be heavy and does not appear as an explicit, dynamical degree of freedom.
- (II) At higher energies, the the pion becomes dynamical and three additional constants

¹In the literature, the isovector, PV πNN coupling is often denoted f_π . Here, however, we adopt the h_π^1 notation to avoid confusion with the pion decay constant.

associated with π -exchange effects appear at lowest order: h_π^1 , along with a second parameter in the EFT potential, k_π^{1a} , and a new meson-exchange current operator characterized by \bar{C}_π . Moreover, the EFT incorporates the effects of two-pion exchange for the first time in a systematic way, leading to predictions for a medium-range component of the PV NN interaction.

The essential differences between the PV EFT and the meson-exchange frameworks – as well as their similarities – are summarized in Figure 1.

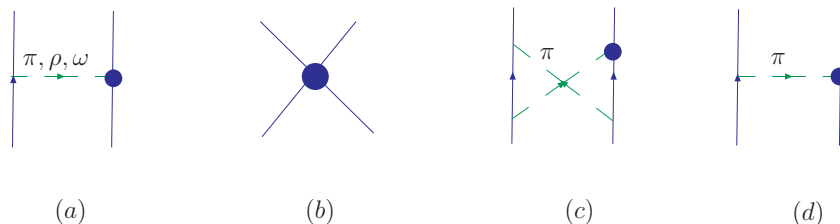


Figure 1: *Comparison of (a) meson-exchange and (b-d) effective field theory (EFT) treatments of the parity-violating NN interaction. Panels (b), (c), and (d) give illustrative contributions to short, medium, and long-range components, respectively .*

Clearly, implementing the EFT approach to the $\Delta S = 0$ HWI requires carrying out new experiments in few-body systems for which ab initio structure computations can be performed. As outlined in Reference (8), a program of such measurements exists in principle. From a practical standpoint, carrying it out will involve meeting a number of experimental challenges. In light of these new theoretical developments and experimental opportunities, we believe it is time to review the field of hadronic PV anew. Comprehensive reviews of the subject have appeared over the years, including the influential Annual Reviews article by Adelberger and Haxton completed two decades ago (9). In what follows, we hope to provide the “next generation” successor to that work, updating the authors’ analysis in light of new theoretical and experimental progress. Since our focus will be on new developments, we touch only lightly on older work that has been reviewed in Reference (9) and elsewhere (10). Before doing so in detail, however, we find it useful to summarize the primary developments and shifts in emphasis that have occurred since Reference (9) appeared:

- The extensive development of χ PT and NN EFT, together with substantial progress in performing lattice QCD simulations, has revolutionized our approach to treating hadronic physics. While the use of hadronic models can provide important physical insights, the present day “holy grail” is to derive first-principles QCD predictions for hadronic phenomena. At the time of the Adelberger and Haxton review, the quark model was still in vogue, whereas lattice QCD and hadronic EFTs had yet to realize their potential. Today, the situation is reversed. Indeed, in the case of $\Delta S = 0$ HWI, the use of a meson-exchange model for the NN interaction that entails a truncation of the QCD spectrum and contains effective couplings that

likely parameterize more physics than the elementary meson-nucleon PV interaction (*e.g.*, 2π -exchange) obscures rather than clarifies the connection with the SM. We now know how to do better.

- New experimental and technological developments have opened the way to performing PV experiments in few-body systems. The landscape now differs substantially from that of the 1980’s, at which time it appeared that measuring a number of $\mathcal{O}(10^{-7})$ effects in few-body processes was impractical. Indeed, two decades ago, the presence of the nuclear enhancement factors made experiments with many-body nuclei such as ^{18}F more attractive than those in few-body systems. Since then, precise new measurements of 10^{-7} PV observables in $\vec{p}p$ scattering, $\vec{n}\alpha$ spin rotation, and polarized neutron capture on hydrogen have either been completed or are in progress, and plans are being developed for other similarly precise few-body measurements at NIST, LANSCE, the SNS, and IASA (Athens). As we discuss below, completion of a comprehensive program of few-body measurements is now a realistic prospect.
- Enormous progress has been made in performing precise, ab initio calculations in the few-body system using Green’s function and variational Monte Carlo methods. These computations start with state-of-the-art phenomenological potentials that incorporate our present knowledge of NN phase shifts and include minimal three-body forces as needed to reproduce the triton binding energy and other three-body effects. A marriage between the NN EFT methods and these few-body computational approaches is also being developed. As a result, a realistic prospect exists for performing precise computations with the PV EFT for few-body observables, leaving one free from the nuclear structure questions that enter the interpretation of many-body PV observables.

In short, the frontier today for understanding the $\Delta S = 0$ HWI lies in the few-body arena, for which a combination of precise experiments and first-principles theory provide new tools for making the most direct possible confrontation with the interplay of the strong and electroweak sectors of the SM. In the remainder of this article, we elaborate on this view.

2 Weak Meson Exchange Model Meets the End of the Road

While the era of the meson-exchange framework for hadronic PV is drawing to a close, it has played such a central role in the field that its development and use following the publication of Reference (9) calls for a brief review. The primary theoretical developments have included updated theoretical “reasonable ranges” and “best values” for the h_M^i provided by DDH and others (6, 11, 12), the analysis of nuclear anapole moments extracted from atomic PV experiments, computations of nuclear PV contributions to PV electron scattering asymmetries, and new global fits of the h_M^i to nuclear and hadronic

PV data. Experimentally, one has seen the completion of the TRIUMF 221 MeV $\vec{p}\vec{p}$ scattering experiment and a neutron spin rotation experiment at NIST, the launching of an $\vec{n}p \rightarrow d\gamma$ experiment at LANCSE, and the first non-zero result for a nuclear anapole moment in an atomic PV experiment with ^{133}Cs .

2.1 Meson Exchange Model of the Weak N-N Interaction

The meson-exchange, PV NN potential, V_{DDH}^{PV} , is generated by the meson-exchange diagrams of Figure 1a, wherein one meson-nucleon vertex is parity conserving and the other parity violating. The Lagrangians for each set of interactions have been written down on numerous occasions in the literature, so we only give the final form of the static potential:

$$\begin{aligned}
V_{DDH}^{\text{PV}}(\vec{r}) = & i \frac{h_\pi^1 g_A m_N}{\sqrt{2} F_\pi} \left(\frac{\tau_1 \times \tau_2}{2} \right)_3 (\vec{\sigma}_1 + \vec{\sigma}_2) \cdot \left[\frac{\vec{p}_1 - \vec{p}_2}{2m_N}, w_\pi(r) \right] \\
& - g_\rho \left(h_\rho^0 \tau_1 \cdot \tau_2 + h_\rho^1 \left(\frac{\tau_1 + \tau_2}{2} \right)_3 + h_\rho^2 \frac{(3\tau_1^3 \tau_2^3 - \tau_1 \cdot \tau_2)}{2\sqrt{6}} \right) \\
& \left((\vec{\sigma}_1 - \vec{\sigma}_2) \cdot \left\{ \frac{\vec{p}_1 - \vec{p}_2}{2m_N}, w_\rho(r) \right\} + i(1 + \chi_\rho) \vec{\sigma}_1 \times \vec{\sigma}_2 \cdot \left[\frac{\vec{p}_1 - \vec{p}_2}{2m_N}, w_\rho(r) \right] \right) \\
& - g_\omega \left(h_\omega^0 + h_\omega^1 \left(\frac{\tau_1 + \tau_2}{2} \right)_3 \right) \\
& \left((\vec{\sigma}_1 - \vec{\sigma}_2) \cdot \left\{ \frac{\vec{p}_1 - \vec{p}_2}{2m_N}, w_\omega(r) \right\} + i(1 + \chi_\omega) \vec{\sigma}_1 \times \vec{\sigma}_2 \cdot \left[\frac{\vec{p}_1 - \vec{p}_2}{2m_N}, w_\omega(r) \right] \right) \\
& - (g_\omega h_\omega^1 - g_\rho h_\rho^1) \left(\frac{\tau_1 - \tau_2}{2} \right)_3 (\vec{\sigma}_1 + \vec{\sigma}_2) \cdot \left\{ \frac{\vec{p}_1 - \vec{p}_2}{2m_N}, w_\rho(r) \right\} \\
& - g_\rho h_\rho^1 i \left(\frac{\tau_1 \times \tau_2}{2} \right)_3 (\vec{\sigma}_1 + \vec{\sigma}_2) \cdot \left[\frac{\vec{p}_1 - \vec{p}_2}{2m_N}, w_\rho(r) \right] . \tag{2}
\end{aligned}$$

Here $\vec{p}_i = -i\vec{\nabla}_i$, with $\vec{\nabla}_i$ denoting the gradient with respect to the coordinate \vec{x}_i of the i -th nucleon, $r = |\vec{x}_1 - \vec{x}_2|$ is the separation between the two nucleons,

$$w_i(r) = \frac{\exp(-m_i r)}{4\pi r} \tag{3}$$

is the standard Yukawa function, and the strong πNN coupling $g_{\pi NN}$ has been expressed in terms of the axial-current coupling g_A using the Goldberger-Treiman relation: $g_{\pi NN} = g_A m_N / F_\pi$, with $F_\pi = 92.4$ MeV being the pion decay constant. The g_V , $V = \rho, \omega$, are the strong vector meson-nucleon Dirac couplings, and the χ_V give the ratio of the strong Pauli and Dirac couplings. The terms in Eq. (2) display different dependences on isospin and spin, so that various observables are sensitive to distinct linear combinations of the h_M^i . A notable feature is the absence of a neutral π -exchange component. Indeed, the only manifestation of π -exchange appears in the first term of Eq. (2) that contains only products of the isospin raising and lowering operators for the two nucleons. This feature reflects a more general theorem by Barton that forbids a neutral pseudoscalar-exchange component in the PV potential when CP is conserved (13).

Table 1: *Theoretical reasonable ranges (second column) and best values (columns 3-5) for the PV meson-nucleon couplings (15), h_M^i , from DDH (6), Dubovic and Zenkin (DZ)(11), and Feldman et al. (12). All values are quoted in units of $g_\pi = 3.8 \times 10^{-8}$.*

PV Coupling	DDH Range	DDH Best Value	DZ	FCDH
h_π^1	0 \rightarrow 30	+ 12	+3	+7
h_ρ^0	30 \rightarrow -81	-30	-22	-10
h_ρ^1	-1 \rightarrow 0	-0.5	+1	-1
h_ρ^2	-20 \rightarrow -29	-25	-18	-18
h_ω^0	15 \rightarrow -27	-5	-10	-13
h_ω^1	-5 \rightarrow -2	-3	-6	-6

The values of the h_M^i appearing in $V_{\text{DDH}}^{\text{PV}}$ are most conveniently expressed in units of g_π , the natural strength for the weak $\Delta S = 1$ $B \rightarrow B'\pi$ couplings²:

$$g_\pi = 3.8 \times 10^{-8} \approx \frac{G_F F_\pi^2}{2\sqrt{2}} \quad . \quad (4)$$

The original DDH reasonable ranges and updated best values are given in Table 1. Note that no prediction for $h_\rho^{1'}$ appears, as DDH were unable to compute this constant in Reference (6). Subsequently, Holstein (14) used a $1/2^-$ pole model to estimate this parameter. Using the quark model to compute the $1/2^- \leftrightarrow 1/2^+$ mixing matrix elements, he obtained $h_\rho^{1'} \simeq 1.8 g_\pi$. Henceforth, we will not refer to this prediction when referring to the DDH values.

The various $\text{SU}(6)_w$ symmetry arguments, current algebra techniques, and quark model estimates that lead to the values in Table 1 have been discussed in detail elsewhere (6, 12), and since our emphasis lies on a new formulation in which these couplings do not appear, we do not revisit those discussions here. Instead, we concentrate on new applications of this framework.

Anapole Effects

Two particularly novel uses of the PV meson-exchange framework have been in the analysis of atomic PV experiments and PV electron scattering. Shortly after PV was observed in μ -decay and β -decay, Zeldovich and Vaks pointed out that weak interactions could also induce a PV coupling of the photon and fermion (16). Electromagnetic (EM) gauge invariance implies that the lowest dimension effective operator for this coupling has the form (17)

$$\mathcal{L}_{\text{PV}}^{ff\gamma} = \frac{F_A}{\Lambda^2} \bar{\psi}_f \gamma_\mu \gamma_5 \psi_f \partial_\nu F^{\mu\nu} \quad , \quad (5)$$

where $F^{\mu\nu}$ is the EM field strength tensor, F_A is the anapole coupling, and Λ is an

²Here, B and B' denote octet baryons.

appropriate mass scale. This effective operator leads to the momentum-space interaction

$$M_{\text{PV}}^{\text{eff}} = -\frac{F_A}{\Lambda^2} \bar{u}(p) \left[q^2 \gamma_\mu - \not{q} q_\mu \right] \gamma_5 u(p) \varepsilon^\mu(q) \quad , \quad (6)$$

where $q = p' - p$ is the momentum of a photon with polarization vector $\varepsilon^\mu(q)$. From (6), it is clear that the anapole coupling involves only virtual photons, since for a real photon $q^2 = 0$ and one can always choose a gauge in which $q \cdot \varepsilon = 0$. Since $\partial_\nu F^{\mu\nu} = J^\mu$, Eq. (5) implies that the anapole interaction effectively couples the fermion axial current to the source of the EM field, J^μ .

In the 1980's, Flambaum, Khriplovich, and Sushkov (18, 19) observed that the anapole moments of nuclei would scale as the square of the nuclear radius, rather than as $1/\Lambda^2$, so that their magnitudes would be enhanced as $A^{2/3}$ in heavy nuclei. Moreover, the nuclear anapole moment would couple the nuclear axial current to the EM currents of the atomic electrons, thereby inducing a PV, nuclear spin-dependent (NSD) term in the atomic Hamiltonian. Experimentally, one could isolate this effect by observing NSD transitions in atomic PV processes. As discussed below, a non-zero result for the ^{133}Cs anapole moment has been obtained by the Boulder group, while limits have been placed on the anapole moment of ^{205}Tl by the Seattle group. Efforts are presently underway to measure the anapole moments of other nuclei, such as francium (for recent reviews, see e.g. references (20, 21, 22)).

The new anapole moment measurements have stimulated considerable theoretical activity. Using a one-body averaged version of $V_{\text{DDH}}^{\text{PV}}$ and a simple single particle shell model, the authors of references (18, 19) estimated the magnitude of the anapole moments of various nuclei, demonstrating the $A^{2/3}$ scaling under these conditions. Substantially more sophisticated shell model calculations – using the complete two-body potential and associated meson-exchange currents – were carried out in references (7, 23, 24). The results have been used to extract constraints on the DDH couplings, as shown in Figure 2. Of particular interest is the significant disagreement between the ^{133}Cs anapole constraints on the relevant isovector combination of couplings, compared with those obtained from the circular polarization P_γ in the γ -decay of ^{18}F . Other nuclear model computations of the ^{133}Cs anapole moment, having greater or lesser degrees of sophistication, lead to similar conclusions (25, 26, 27, 28, 29, 30).

As discussed in references (7, 24), state-of-the art shell model computations unavoidably entail model-space truncations, and in the case of the cesium anapole moment calculations, inclusion of the omitted contributions would likely increase, rather than decrease, the disagreement with the ^{18}F result. In contrast, the nuclear structure analysis used to interpret the P_γ results is thought to be robust, since the dominant nuclear mixing matrix element can be calibrated against an analog β -decay amplitude (31, 32). Thus, the implications of the new result for the Cs anapole moment are quite puzzling.

The $\Delta S = 0$ HWI can also contribute to the PV asymmetry A_{PV} measured in the scattering of longitudinally polarized electrons from hadronic and nuclear targets. In the late 1990's, it was realized that the anapole moment of the proton contributes to A_{PV} for elastic $\vec{e}p$ scattering in a way that is indistinguishable from that of the axial vector coupling of the Z^0 to the proton, or G_A^e (see Figure 3) (33). Moreover, it was shown – using the DDH framework – that the both the magnitude of the proton anapole moment

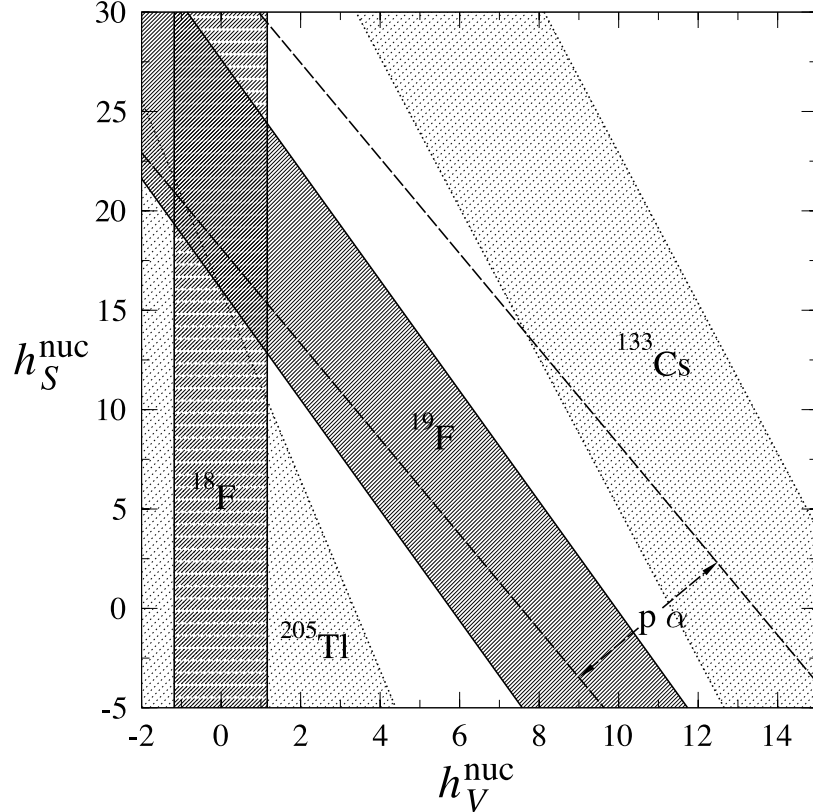


Figure 2: Constraints on effective DDH weak meson-nucleon couplings deduced from PV observables in nuclei and anapole moments of heavy atoms (courtesy of W. C. Haxton). Here, $h_V^{\text{nuc}} = h_\pi^1 - 0.12h_\rho^1 - 0.18h_\omega^1$ and $h_S^{\text{nuc}} = -(h_\rho^0 + 0.7h_\omega^0)$

contribution as well as the theoretical uncertainty associated with it was sufficiently large as to significantly affect the interpretation of A_{PV} . At that time, a program of PV electron scattering measurements was being developed to determine the strange quark contributions to the electric and magnetic form factors of the proton, G_E^s and G_M^s , respectively. The presence of the anapole related uncertainties would be particularly problematic for the extraction of G_M^s from the backward angle asymmetry measurements (34, 35).

Consequently, additional measurements of A_{PV} for quasielastic (QE) scattering from the deuteron were carried out. Since the deuterium asymmetry is strongly sensitive to G_A^e but considerably less sensitive to G_M^s than is the proton asymmetry, a measurement of $A_{\text{PV}}^{\text{QE}}(\vec{e}D)$ – in conjunction with $A_{\text{PV}}^{\text{El}}(\vec{e}p)$ – could be used to test the theoretical estimates of Reference (33) while providing for a determination of G_M^s that is independent of hadronic PV uncertainties. The initial results of these measurements, completed by the SAMPLE Collaboration (36), yielded a new puzzle: the effective G_A^e extracted from the $\vec{e}p$ and $\vec{e}D$ asymmetries was consistent with zero. The calculations of Reference (33) had predicted a $\sim 40\%$ reduction to the value of G_A^e arising from SM electroweak radiative corrections and the anapole effect. The SAMPLE result, however, implied a substantial

enhancement of the anapole contribution or that of other radiative corrections over the predictions of Reference (33).

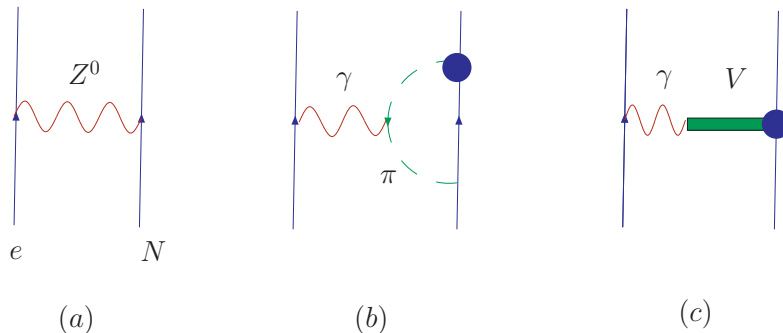


Figure 3: Contributions from hadronic PV (proton anapole moment) to the effective axial vector electron-proton coupling, G_A^e .

Subsequent theoretical studies attempted to determine the origin of the anomaly, scrutinizing various contributions to A_{PV} : the original computation of Reference (33) was revisited and updated using heavy baryon χ PT (37); possible quark model enhancements were considered (38); the q^2 -dependence of the anapole contribution was studied (39, 40), and contributions from parity mixing in the deuteron and final np states were computed using the meson-exchange model (41, 42). In all cases, no large effects were found that could resolve the puzzle. Ultimately, the SAMPLE Collaboration carried out a reanalysis of the pion-production background in the deuterium experiment that shifted the value of $A_{\text{PV}}^{\text{QE}}(\vec{e}D)$ (43) and brought the axial term into agreement with the predictions of references (33, 37). The theoretical results from the latter work have now been used in extracting G_M^s from the backward angle proton asymmetry (44).

Within the DDH framework, these developments – along with the completion of a new $\vec{p}p$ scattering experiment at TRIUMF – have motivated reanalyses of the hadronic and nuclear PV observables in terms of the h_M^i . After discussing the recent experimental developments, we provide a summary of our current understanding of hadronic PV in this context and make the case that a fundamental paradigm shift is required in order to make further progress in this field.

2.2 Experimental Progress

Earlier reviews, e.g. (9), (15), (45), have documented an extensive body of experimental work aimed at characterizing the $\Delta S = 0$ HWI, largely carried out in many-body nuclei. As noted in the Introduction, the PV effects in the much simpler NN and few nucleon systems were almost impractically small [$\mathcal{O}(10^{-7})$] from the standpoint of past experimental feasibility, so the realization of fortuitous nuclear structure effects that ‘amplify’ the underlying NN PV signal by several orders of magnitude naturally led to an earlier

focus on many-body systems. Future progress will hinge on a handful of precise experiments in much simpler few nucleon systems, for which the theoretical interpretation is less fraught with model-dependent uncertainties and for which precise measurements now appear to be realistic. Here, we review recent experimental progress in the few-body sector and comment on new developments in probes of PV in many-body nuclei. These developments have been cast largely in the weak meson-exchange framework, so we will use it here in discussion their theoretical implications. When developing the EFT framework in Section 3, we will reframe the discussion of these theoretical implications in the EFT formulation.

Probing the NN weak interaction in few body systems presents significant experimental challenges. The bare NN $\mathcal{O}(10^{-7})$ PV effects compete with a host of potential systematic errors at this level, which must be both minimized through careful experimental design and simultaneously measured to ensure that they do not obscure the true PV signal. Even acquiring sufficient data to reach a statistical error at the $10^{-7} - 10^{-8}$ level is no mean feat, necessitating the use of current mode detection which in turn introduces its own systematic error sensitivities that must be controlled and understood. The most accessible NN and few nucleon observables are accessed in polarized beam experiments, where rapid polarization reversal provides a practical means of suppressing low frequency noise and systematic effects, at the expense of introducing a built in sensitivity to spin correlated beam properties that can mimic the PV observable in question. In such cases, as much effort must be expended to optimize and characterize the polarized beam properties as is required to design and commission the PV experimental apparatus. Typically, a successful experiment spans a decade or more from initial concept to publication of a significant result, with continuous refinements of the experimental apparatus and technique until the desired sensitivity is reached. In most cases, an order of magnitude more data are required to refine and test the apparatus than to acquire the final PV data sample.

To date, there have been a number of significant measurements of PV in pp scattering, but despite several decades of experimental effort, a definitive observation of PV in the np system remains to be established. Recent experimental progress in the NN system includes the completion of a program of high precision measurements of PV in pp scattering which yield independent constraints on the weak couplings of heavier mesons, and commissioning of a PV asymmetry measurement in $\vec{n}p \rightarrow d\gamma$ that is aimed at a precise determination of h_π^1 . These experiments will be discussed briefly below; future possibilities for precise measurements in two and few-nucleon systems are discussed in Section 3.

2.2.1 Longitudinal Analyzing Power in pp Scattering

The PV observable that has been studied in pp scattering is the longitudinal analyzing power, $A_z = \frac{(\sigma^+ - \sigma^-)}{(\sigma^+ + \sigma^-)}$, where σ^+ and σ^- are the elastic scattering cross sections for positive and negative helicity beams incident on an unpolarized hydrogen target. The analyzing power can be naturally expressed as a sum of parity mixed partial wave contributions, with only $S - P$ mixing required to characterize A_z at low energy. The first two partial waves in the expansion are sufficient to describe A_z up to several hundred MeV;

the ($^1S_0 - ^3P_0$) contribution dominates at low energy, while the ($^3P_2 - ^1D_2$) amplitude starts to become significant above 100 MeV. These two partial wave amplitudes have complementary dependences on the weak M-N couplings: $h_\rho^{pp} = (h_\rho^0 + h_\rho^1 + h_\rho^2/\sqrt{6})$ and $h_\omega^{pp} = h_\omega^0 + h_\omega^1$. As noted by Simonius (46), the dominant $S - P$ wave mixing integrates to zero near 220 MeV beam energy, due to a fortuitous cancellation of the strong S and P wave phase shifts. This observation motivated the recently completed TRIUMF experiment at 221 MeV (47), which was designed to isolate ($^3P_2 - ^1D_2$) contribution.

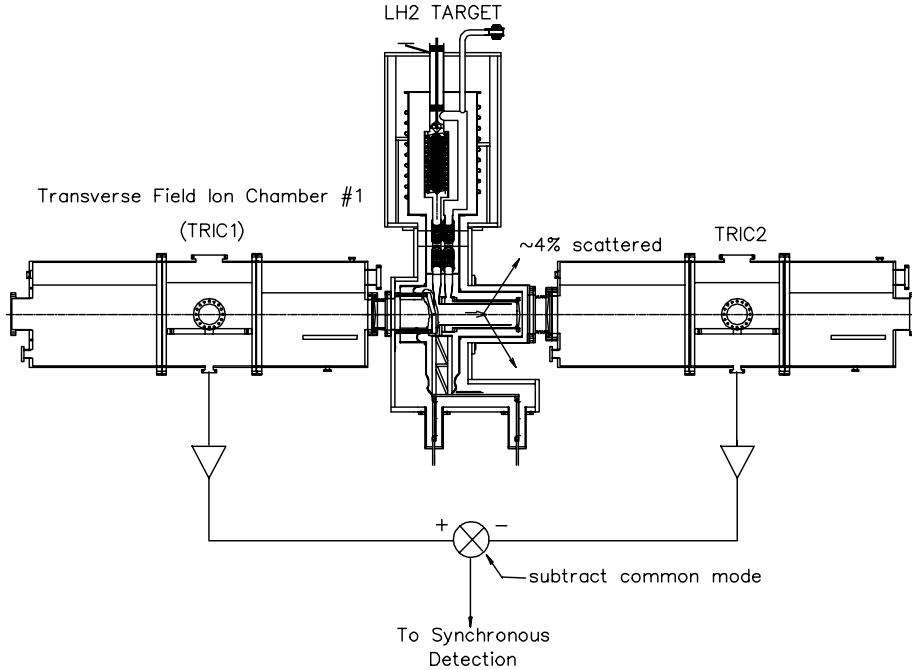


Figure 4: *Principle of the TRIUMF p - p parity violation experiment. Longitudinally polarized protons at 221 MeV passed through a 40 cm liquid hydrogen target, which scattered $\simeq 4\%$ of the beam. The polarization-dependent target transmission was measured by performing an analog subtraction of two dc current signals from transverse field ionization chambers. Reprinted with permission from Berdoz et al., *Phys. Rev. C* Vol. 68, 034004 (2003), Fig. 1. Copyright (2003) by the American Physical Society.*

While earlier high precision measurements at low energy were performed in a total scattering geometry, the TRIUMF 221 MeV measurements were carried out in transmission mode. The small size of the total scattering asymmetry $A_z \simeq 10^{-7}$ implied a transmission asymmetry of order 10^{-9} for the TRIUMF experiment. Integrating detectors with small angular acceptance coupled to low noise electronics, excellent beam and liquid hydrogen target stability, and a highly polarized beam with minimal helicity correlated beam properties were essential to the success of the measurements. Rapid beam polarization reversal (40 Hz, with controlled phase slip with respect to the line frequency) led to an ac parity violating signal at a well determined frequency, greatly suppressing the noise contributions with respect to a dc measurement (which would be impossible in this case due to the extremely small size of the parity violating asymmetry signal). The principle of the TRIUMF transmission mode measurement is illustrated in Figure 4.

The TRIUMF laboratory spent many years developing a state-of-the-art optically pumped polarized H- ion source (OPPIS) (48, 49), which was ideal for demanding symmetry tests that require polarized beam, since the polarization ($\simeq 85\%$) was reversed by changing the frequency of the laser light with no changes to macroscopic electric or magnetic fields that could influence the beam properties. Even so, significant corrections ($\simeq 40\%$) had to be made to the raw asymmetry for helicity correlated transverse polarization components.

Transverse polarization is a pathological source of systematic error in pp scattering measurements because of the relatively enormous parity-allowed transverse analyzing power A_y , which is over a million times larger than the PV longitudinal analyzing power A_z . While it is not practical to demonstrate and maintain tiny transverse polarization components at or below the 10^{-6} level, fortunately the geometrical symmetry of the apparatus can be invoked to establish a ‘neutral axis’ for the beam transport such that the false asymmetry arising from transverse polarization components is identically zero if the beam is locked on this axis by a position feedback system. This technique was used to ensure that corrections for average transverse polarization components $\langle P_y \rangle$ and $\langle P_x \rangle$ were insignificant at the 10^{-9} level in the TRIUMF measurements – the associated corrections ΔA_z e.g. for transverse vertical polarization $\langle P_y \rangle$ scale as $\langle x \rangle \langle P_y \rangle$, where $\langle x \rangle$ is the net displacement from the symmetry axis, whose location can be determined by separate calibration experiments. Note that the form of the driving term $\langle x \rangle \langle P_y \rangle$ is that of the first moment of transverse polarization at the detector location, which is referred to as an extrinsic first moment; a similar correction must also be made for intrinsic first moments of the form $\langle x P_y \rangle$ which arise from nonuniform distributions of transverse polarization within the beam envelope. These extrinsic polarization moments are extremely difficult to measure and control.

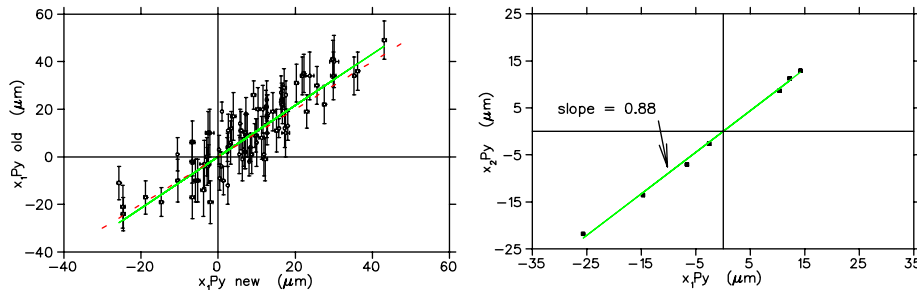


Figure 5: *Demonstration of a new current mode scanning polarimeter at TRIUMF. Left panel: intrinsic polarization moments $\langle xP_y \rangle$ measured simultaneously with counting mode (vertical axis) and current mode (horizontal axis) devices. The errors on the current mode measurements are too small to display on this scale. The dotted line has a slope of unity, and the solid line is a fit to the data. Right panel: intrinsic polarization moments for a given beamline tune, measured with a pair of current mode PPMs. The ratio of moments at PPM1 and PPM2 remains relatively constant, thus verifying an essential assumption of the systematic error reduction scheme. Reprinted with permission from Ramsay et al., Proc. 9th International Workshop on Polarized Sources and Targets, p. 289-293 (2002), Fig. 3. Copyright (2002) by World Scientific.*

In the TRIUMF experiment, a pair of scanning polarimeters (50) was employed to provide continuous measurements of the distribution of transverse polarization components within the beam, interleaved with parity data taking from the transverse ion chambers on an 8-state, 200 ms data cycle. The limiting factor in the TRIUMF experiment was the statistical precision of the PPMs, which were coincidence counting mode devices. An essential assumption made in determining the correction for intrinsic polarization moments was that the moments evolved linearly with position along the beamline and thus had a stable ratio between upstream and downstream PPMs. This ratio could in principle be tuned to achieve a null sensitivity to intrinsic polarization moments, an approach modelled on the successful polarization neutral axis idea described above. Unfortunately, the ability of the PPMs to measure this first moment ratio sufficiently precisely in a reasonable amount of time was severely limited, and so significant corrections still had to be made to the data.

R & D efforts towards a follow up experiment at higher energy (which was never realized) included development of a current mode scanning polarimeter which had $\sim 20\times$ greater statistical precision (51); the current mode polarimeter was able to clearly demonstrate the constant linear evolution of intrinsic moments along the beamline, as illustrated in figure 5, thus independently validating the corrections procedure that was used to obtain a final result for A_z at 221 MeV from TRIUMF experiment 497.

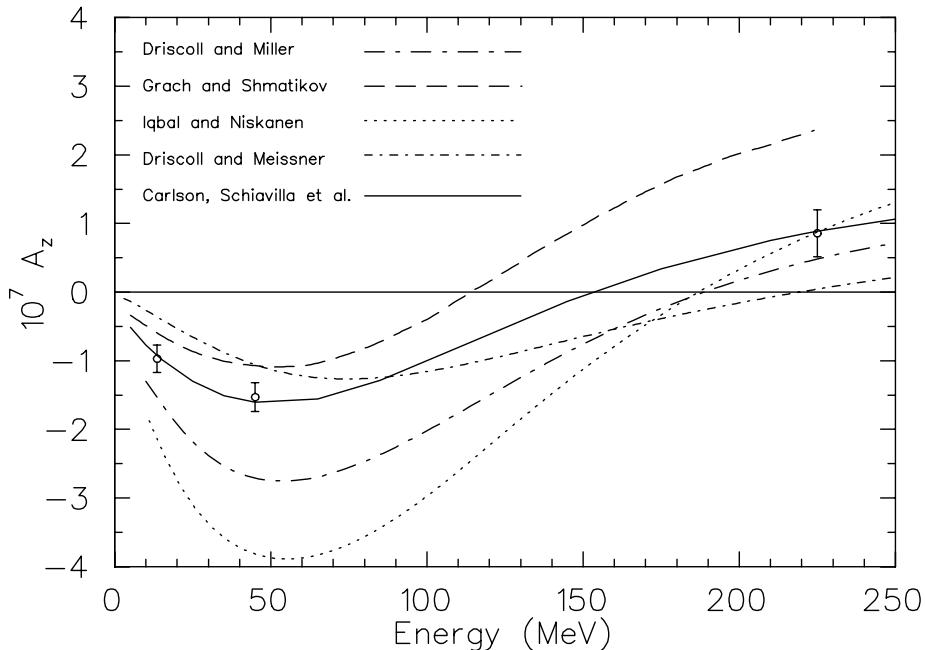


Figure 6: *The most precise measurements of parity violation in pp scattering at low and intermediate energy, and recent theoretical predictions. Experiments were performed at Bonn (13.6 MeV) (52), PSI (45 MeV) (53) and TRIUMF (221 MeV) (47). The solid curve shows the calculation by Carlson et al. (54) including a fit of the weak meson-nucleon coupling constants to the data. Reprinted with permission from Berdoz et al., Phys. Rev. C Vol. 68, 034004 (2003), Fig. 13. Copyright (2003) by the American Physical Society.*

Parity violation in pp scattering has attracted considerable theoretical interest since the review of Reference (9). Recent calculations are shown in Figure 6 together with the most precise experimental data at low and intermediate energies. Driscoll and Miller (55, 56) used the Bonn potential to treat the strong NN interaction, with weak meson-nucleon couplings taken from Reference (6). Iqbal and Niskanen's calculation adds a Δ isobar contribution (57) to the Driscoll and Miller model. The calculation of Driscoll and Meissner (58) is based on a chiral soliton model, while the quark model calculation of Grach and Shmatikov (59) takes explicit account of quark degrees of freedom.

Figure 7 by Carlson et al. (54) shows the limits on the weak meson-nucleon couplings h_ρ^{pp} and h_ω^{pp} imposed by the low energy pp asymmetry measurements and the 221 MeV TRIUMF result. The error bands are based on a calculation assuming the Argonne v_{18} (AV-18) potential (60), the Bonn 2000 (CD-Bonn) (61) strong interaction coupling constants, and including all partial waves up to $J=8$. Although the TRIUMF measurement is not sensitive to A_z from SP mixing, and the contribution from PD mixing contains no h_ω^{pp} contribution, there is some h_ω^{pp} dependence arising from higher partial waves. The best fit to the pp data yields $h_\rho^{pp} = -22.3 \times 10^{-7}$ and $h_\omega^{pp} = 5.17 \times 10^{-7}$, compared to the DDH "best guess" values of $h_\rho^{pp} = -15.5 \times 10^{-7}$ and $h_\omega^{pp} = -3.0 \times 10^{-7}$.

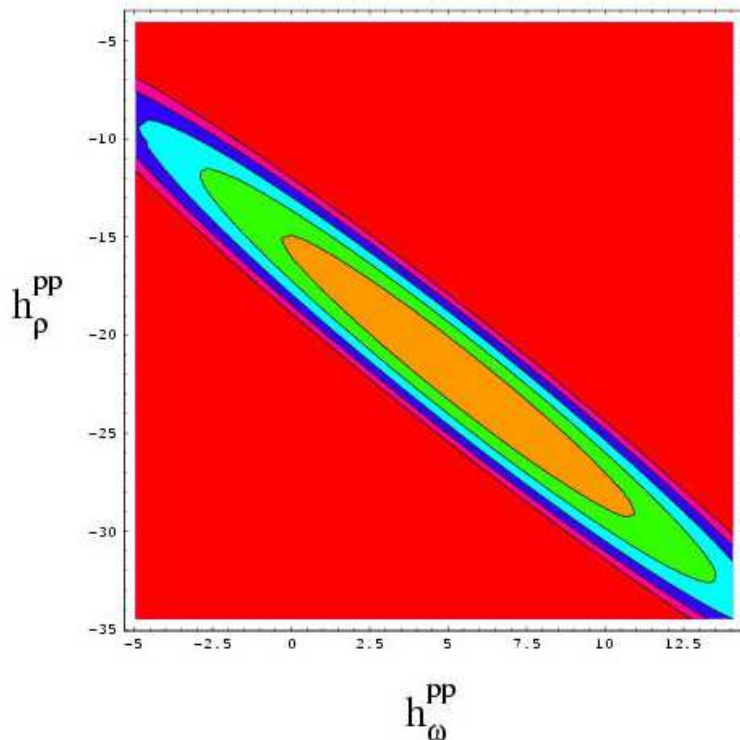


Figure 7: Present constraints on the weak meson-nucleon couplings h_ρ^{pp} and h_ω^{pp} , fitted to the low energy and 221 MeV pp asymmetry data (54). The plot shows curves of constant total $\chi^2 = 1, 2, 3, 4$ and 5. Axis scales are 10^{-7} . Reprinted with permission from Carlson et al., *Phys. Rev. C* Vol. 65, 035502 (2002), Fig. 8. Copyright (2003) by the American Physical Society.

2.2.2 Progress in the np System

Parity violation in the np system can in principle be detected in a variety of processes that can reveal complementary aspects of the weak NN interaction. In np capture, there are two complementary PV observables: P_γ^d , the 2.2 MeV γ ray circular polarization for an unpolarized neutron beam, and A_γ^d , the asymmetry in the emission of γ rays with respect to the neutron spin direction if the beam is polarized. Closely related to the first of these, P_γ^d , is the helicity asymmetry A_L^γ in the photodisintegration of deuterium with circularly polarized photons; the two are asymptotically equal to each other at threshold, while A_L^γ is predicted to drop rapidly with increasing photon energy, falling an order of magnitude as the photon energy increases to 1 MeV above threshold (62). Finally, the transmission of polarized neutrons through hydrogen should reveal a tiny PV spin rotation about the neutron propagation direction \hat{z} : $d\phi^{np}/dz$.

Unfortunately, all of these np system measurements are extremely challenging; the first three have been attempted (63, 64, 65) but have yielded null results with limits at least one order of magnitude too large to provide a meaningful constraint on the weak meson-exchange predictions (62, 66, 67, 68, 69) all of which are at the level 5×10^{-8} or smaller. The two PV observables involving the np capture reaction, P_γ^d and A_γ^d have complementary dependences on the weak MN couplings – notably, A_γ^d can yield a unique constraint on h_π^1 , while P_γ^d depends on a linear combination of π , ρ and ω weak couplings (9). Measurement of gamma ray circular polarization requires a Compton polarimeter with typical sensitivity at the few percent level, thus rendering the P_γ^d measurement in principle even more challenging than a measurement of A_γ^d . A measurement of the helicity asymmetry A_L^γ in the photodisintegration of deuterium is at the early conceptual design stage for the future experimental program at IASA, Athens (70), with the aim of reaching a sensitivity at the 10^{-8} level. The np spin rotation measurement, with an anticipated $d\phi^{np}/dz = 5 \times 10^{-7}$ rad/m (71) has not yet been attempted, but is envisioned as a future component of the SNS fundamental neutron physics program, as discussed in Section 3.4 below.

The intrinsic interest of a clean measurement of h_π^1 in the NN system, together with considerations of experimental feasibility, have led to the launching of a major effort at LANSCE (72) – the NPDGamma experiment – to make a definitive measurement of A_γ^d , with an ultimate goal of reaching $\pm 10\%$ of the DDH prediction. The measurement of A_γ^d requires a polarized neutron beam with precisely known spin direction and a measurement of the 2.22 MeV gamma ray angular distribution: $\frac{d\omega}{d\theta} \sim (1 + A_\gamma \cos\theta)$, where θ is the angle between the gamma ray momentum and the neutron spin. Even at milli-eV neutron energies for neutrons moderated in liquid hydrogen, the scattering cross section exceeds the capture cross section by a significant factor. A parahydrogen target is essential to avoid neutron spin flip on scattering in the target, and the useful beam flux is below 15 meV to prevent depolarization in the target.

A previous measurement of A_γ^d , performed at the ILL reactor in the 1970's (65) reported a value of $(0.6 \pm 2.1) \times 10^{-7}$; the NPDGamma experiment is designed to reach an ultimate sensitivity of $\pm 5 \times 10^{-9}$, with the uncertainty dominated by statistical rather than systematic errors. Major improvements in the experimental instrumentation and techniques that should make this possible include:

- use of a high intensity, low energy, pulsed beam, which allows for neutron energy determination via time-of-flight measurement and allows for a separation in time of prompt γ ray background from the neutrons of interest;
- polarization of the beam via selective transmission through optically pumped polarized cells of ^3He ; the well known spin-dependent cross section leads to an energy dependent polarization that can be very high for low energy neutrons, and the beam polarization can be continuously and directly monitored by online measurements of the ^3He cell transmission;
- use of a resonant RF spin flipper capable of flipping spins at all neutron energies with high efficiency and eliminating Stern-Gerlach steering of the neutron beam associated with spin flip;
- implementation of a large solid angle, high efficiency CsI (Tl) gamma detector array (73) instrumented with sensitive current mode electronics whose intrinsic noise is negligible compared to neutron counting statistics.

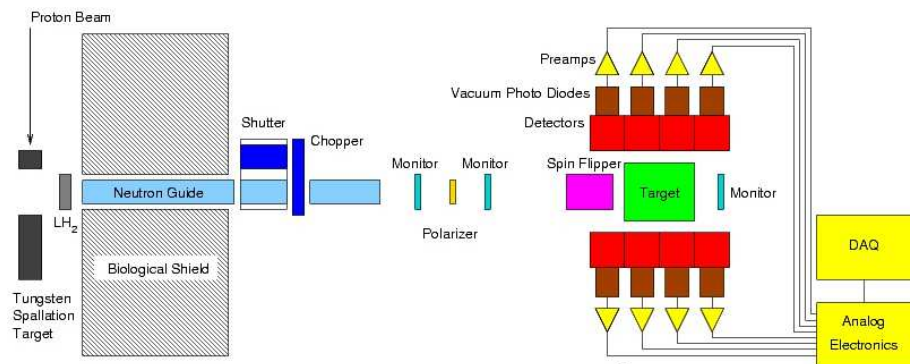


Figure 8: *Layout of the NPDGamma apparatus currently taking data on Flight Path 12 at LANSCE. A highly uniform, vertical magnetic guide field to preserve the neutron spin direction is provided by a set of field coils (not shown).*

A schematic of the NPDGamma apparatus mounted in the new experimental cave on flight path 12 at LANSCE is shown in Figure 8. The neutron spins, polarized by the ^3He transmission cell, are efficiently reversed by the RF spin flipper on a pulse-by-pulse basis, thus alternating the sign of the parity violating asymmetry measured in the gamma detector array at 20 Hz. At the time of writing, NPDGamma has achieved a number of major milestones and is ready to take production data at LANSCE, pending installation of the liquid hydrogen target. The apparatus has been fully commissioned; electronic asymmetries are consistent with zero at the few $\times 10^{-9}$ level, and PV asymmetries arising from neutron capture on a variety of solid targets which are representative of materials used to construct the beamline and parity instrumentation have been measured. All are consistent with zero at the 10^{-6} level or smaller, with sufficient accuracy to conclude that background asymmetries will not play a significant role in the hydrogen target data. A known PV asymmetry in Cl at the 10^{-5} level has been remeasured and

will be used as a diagnostic tool for NPDGamma, with the periodic insertion of a CCl_4 target to verify the consistent performance of the experimental setup. Contamination of the hydrogen target PV (up-down) asymmetry by the comparably small, parity-allowed left-right asymmetry will be kept below an acceptable level by determining the effective detector angles in situ – this in turn will be accomplished by scanning the detector array horizontally and vertically with respect to the target while acquiring np capture data. The measured chlorine asymmetry is shown in figure 9; the net PV (up-down) and parity-allowed left-right asymmetries deduced from these data (72) are: $A_\gamma = (-19 \pm 2) \times 10^{-6}$ and $A_{LR} = (-1 \pm 2) \times 10^{-6}$.

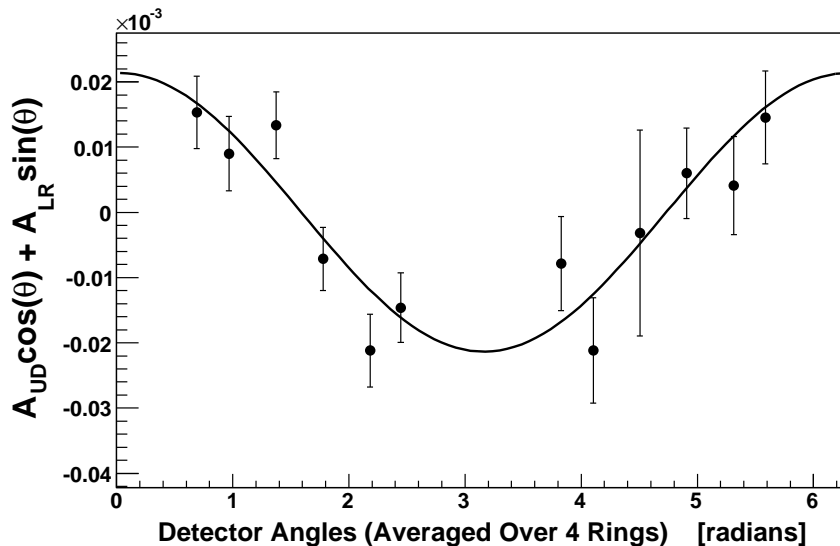


Figure 9: CCl_4 gamma ray asymmetries, calculated from opposing detector pairs, plotted versus angle of the first detector in the pair with respect to the vertical, for the NPDGamma 2004 data. The total asymmetry $A = A_\gamma \cos\theta + A_{LR} \sin\theta$ is deduced from the fit. Figure courtesy of M. T. Gericke.

Unfortunately, a number of factors have conspired that severely limit the statistical accuracy that can be achieved by running the NPDGamma experiment at LANSCE. These include a factor of 4 reduction in the available neutron flux per beam pulse as compared with expectations prior to the recent upgrade of the LANSCE facility, and a further reduction in high quality beam time due to magnetic interference from a neighboring experiment. In view of these limitations, the NPDGamma collaboration plans to carry out a first measurement with hydrogen in 2005-2006, which would provide a statistics limited result for A_γ^d accurate to $\pm 1 \times 10^{-7}$ or better. At the time of writing, plans are being made to move the experiment to the Fundamental Neutron Physics Beam Line at the Spallation Neutron Source, which would enable the collaboration to make a measurement of A_γ^d to $\pm 1 \times 10^{-8}$ or better, as discussed in Section 3.4.

2.2.3 Neutron Spin Rotation Experiments

Low energy neutrons can exhibit a parity violating spin rotation induced by the hadronic weak interaction as they pass through a medium. The observable, ϕ_{PV} , is the angle of transverse spin rotation about the neutron's direction of motion. In the limit of zero neutron energy, the PV neutron spin rotation is energy independent (74). After traversing a distance z through the medium, the neutron spin will precess by an amount $\phi_{PV} = 2\pi\rho z f_{PV}$, where f_{PV} is the parity violating coherent forward scattering amplitude for a low energy neutron and ρ is the number density of the medium (75). The basic requirements of a neutron spin rotation experiment are a source of low energy polarized neutrons, a target containing the material of interest, and a spin analyzer downstream of the target, from which the value of ϕ_{PV} can be deduced.

Two cases are particularly interesting from the standpoint of testing models of the hadronic weak interaction: parity violating neutron spin rotations in ^1H and ^4He . These two cases have complementary dependences on the weak meson-nucleon couplings. The np case is dominated by the weak pion exchange contribution, and thus would yield similar information to the NPDGamma experiment described above. The ^4He PV spin rotation has a significant contribution from h_π^1 but is also sensitive to the h_ρ^0 coupling. Experimentally, the ^4He case is more tractable, due to a much longer mean free path for low energy neutrons than hydrogen. Like NPDGamma, the np spin rotation experiment would require a parahydrogen target to avoid neutron depolarization due to spin-exchange collisions with the hydrogen molecules, and only neutron energies below 15 meV would be useful for the experiment.

A ^4He spin rotation measurement was carried out at NIST in the 1990's (76), with the result: $\phi_{PV} = (8 \pm 14_{stat} \pm 2_{sys}) \times 10^{-7}$ rad/m. Unfortunately this heroic effort did not reach sufficient sensitivity to test hadronic weak interaction models. A possible experiment in hydrogen has been considered but not yet proposed, and will hopefully be carried out at the SNS within the next decade (see Section 3.3).

What confounds the beautiful simplicity of the measurement principle is the extremely small size of the PV rotations expected based on the DDH model: for ^4He , the predicted effect is $\phi_{PV} = -1 \times 10^{-7}$ rad/m (77), while for the proton, the effect should be about 5 times larger (71). These PV spin rotations are 8 orders of magnitude smaller than those induced by the earth's magnetic field in a typical measurement apparatus! Therefore, a much more elaborate scheme is required in order to achieve the necessary sensitivity. Great care must be taken to reduce ambient magnetic fields by many orders of magnitude; residual fields must be monitored carefully, and the experiment should be designed so that the effects of residual magnetic fields are cancelled to the maximum possible extent in the extraction of the PV spin rotation angle.

The basic experimental technique employed at NIST and foreseen for subsequent measurements involves a double beam / double cell apparatus, as sketched in Figure 10. The double cell design incorporates a 180° spin precession about the initial spin direction between the two target cells, one of which is full and one empty, for a given measurement. A clear advantage of the double cell design is that the much larger spin rotations due to residual magnetic fields exactly cancel in the two target states, to the extent that the magnetic fields and the neutron trajectories are exactly the same in both cases. An

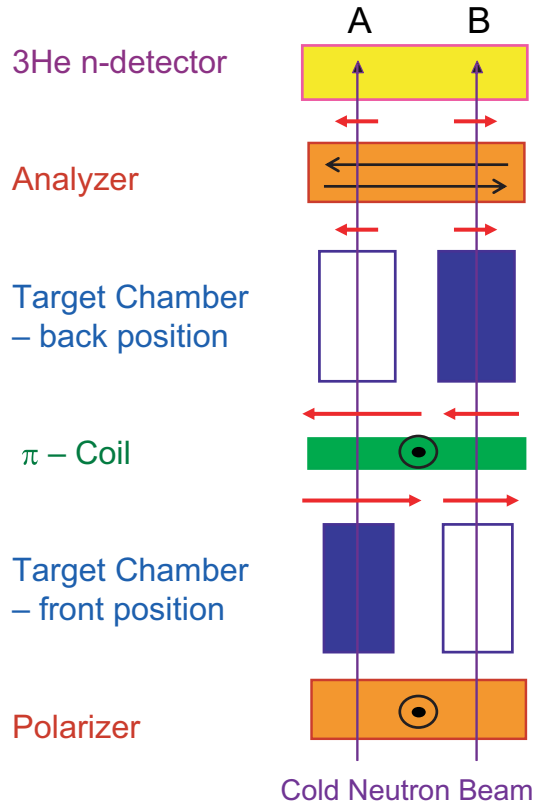


Figure 10: *Schematic of the double beam / double target system for ^4He neutron spin rotation measurements. The incident neutron spins are polarized out of the page. The PV effect is a spin precession around the direction of motion, which leads to components in the horizontal plane as shown. Either the front or the back target is full (shaded), and the other is empty, in channels A and B. Much larger spin rotations due to local magnetic fields are independent of the target state and are cancelled by subtraction. The π coil situated between the front and rear targets precesses the neutron spin by 180° about the initial spin direction, thus reversing the sign of the PV spin rotation relative to that due to magnetic fields, indicated in the figure; the counting rate $(B - A) = 2 \phi_{PV}$. (Figure courtesy of Anna Micherdzinska)*

identical double target system sits beside the first one in the same cryostat, half the beam passes through each, and the two systems are run so that at any given time, the sign of the PV spin rotation in the two subsystems is exactly opposite. Downstream of the double target system is a polarization analyzer and segmented ^3He ionization chamber which measures the counting rate in ‘left’ and ‘right’ elements of the apparatus simultaneously.

Instead of rapidly flipping the beam polarization as in the pp and NPDGamma experiments described earlier, the sign of the PV effect is reversed by alternating the location of the full target cell with respect to the π coil. The emptying and filling of the target cells took several minutes in the first spin rotation experiment, and each measuring interval was 10 min, corresponding to a reversal rate of 1 mHz and roughly 25% dead time. However, with a pair of double cell setups located side by side in the same cryostat,

and a beam splitter upstream of the apparatus, reactor beam intensity fluctuations can be effectively cancelled, which makes up for the slow PV reversal frequency.

Features of the upgraded apparatus include: improved magnetic shielding, resulting in a fourfold reduction of ambient fields to the 20 μG level; improved cryogenic systems with a faster target cycling time; operation with superfluid ^4He , which has a much smaller total and small-angle neutron scattering cross section than normal ^4He , and improvements to the NIST cold source leading to a 50% increase in the beam fluence. These and other improvements should result in a statistical error of $\pm 3 \times 10^{-7}$ rad/m in a 3 month run at NIST during 2005-06, with systematic errors (based on simulations of the experiment) at the 10^{-8} level. Like NPDGamma, the collaboration proposes to move the ^4He spin rotation experiment to the SNS, where the high intensity pulsed cold neutron beam would permit a high statistics measurement in about a year's running time with greater diagnostic capability for systematic errors (78).

2.2.4 Nuclear Anapole Moments

Nuclear anapole moments, which may be accessed via measurements of parity violation in atoms, have recently opened a new window on the hadronic weak interaction (79). This subject has been the focus of significant theoretical and experimental effort, including a recent review article in this journal (20). A detailed discussion of experimental atomic physics approaches is beyond the scope of the present work; however, for completeness, we include a brief overview of experimental efforts here.

A prime motivation for atomic PV measurements is to provide stringent tests of the electroweak Standard Model. The dominant contribution to the neutral weak electron - nucleus interaction arises from an axial coupling to the electron and a vector coupling to the nucleus and is proportional to the nuclear weak charge, Q_W . The value of Q_W can be computed with high accuracy in the SM, and a precise experimental determination of the nuclear weak charge can probe for deviations that one might expect to arise from physics beyond the SM. This dominant PV contribution is nuclear spin independent, and the extraction of Q_W is minimally affected by hadronic weak interaction corrections. However, the weak electron - nucleus interaction also has a contribution from the vector coupling of the electron to the axial current of the nucleus; this leads to a nuclear spin dependent (NSD) parity violating interaction that can be detected as a small hyperfine dependence of atomic PV. The parity violating interaction in this case has contributions from Z^0 exchange, a hyperfine interaction correction, and finally the nuclear anapole moment (7, 24).

The weak interaction typically induces very tiny opposite-parity wavefunction admixtures in atomic states, on the order of 10^{-11} . These in turn give rise to extremely small and otherwise parity-forbidden transition amplitudes. The best explored case is atomic PV in Cs, measured in the highly forbidden 6s-7s transition in an atomic beam, where the tiny PV amplitude was arranged to interfere with a much larger Stark-induced transition amplitude in the presence of a static E field.³ The authors (79) report the use

³The advantage of this seemingly complicated experimental scheme is that the interference technique yields an observable which is linear in the tiny PV amplitude, rather than trying to measure the forbidden transition rate, which is quadratic.

of 31 different servo systems to precisely control electrical, optical and mechanical systems during the measurements; they designed an experiment with 5 independent means of reversing the parity signal, and spent about 20 times more data taking effort in the investigation and elimination of systematic errors compared to actual PV data taking. From the standpoint of atomic structure calculations needed to interpret the measurements, the heavy alkali atom Cs is ideal for precision PV studies, due to its relatively simple electronic configuration of one valence (6s) electron outside a tightly bound Xe noble gas core.

Since the nuclear anapole contribution is expected to scale as $A^{2/3}$, and the atomic PV signature used to detect it scales as $Z^{\frac{2}{3}}$, heavy nuclei are the preferred systems for experimental studies. To date, a definitive experimental result exists only for the anapole moment of ^{133}Cs (79), while an upper limit has been obtained for the anapole moment of Tl (30% ^{203}Tl , 70 % ^{205}Tl isotopic ratio) (80) obtained via PV optical rotation measurements. In Cs, the nuclear spin independent atomic PV effect has been measured to 0.4%, while the anapole moment contribution has been determined to 14%. In Tl, the spin independent effect has been measured to 3%, and the spin dependent anapole contribution is consistent with zero. These are the result of truly heroic experimental investigations spanning over a decade of instrumentation development and testing. Interpretation of the spin independent PV as a Standard Model test requires excellent understanding of the atomic structure, while the anapole moment must be first unravelled from the competing effects of Z^0 exchange and a hyperfine correction, and then interpreted in terms of a HWI model, e.g. the meson-exchange model of DDH.

Atomic PV has been measured in other systems, but to lower precision than in Cs, and with greater uncertainty in the atomic structure details needed to interpret the measurements. Currently, a new generation of experiments is under development, aimed at determining both the nuclear spin independent and anapole moment contributions to high precision. This includes ongoing efforts to develop alternative experimental approaches to atomic PV measurements in Cs; demonstration of a new technique based on stimulated emission has recently been reported (81), anticipating that an ultimate precision of 0.1% could be reached. As remarked in (82), there is a significant advantage to measuring PV in a range of isotopes of the same atom, since a number of atomic structure uncertainties cancel when PV ratios are considered. Atomic ytterbium ($Z=70$), having 7 stable isotopes, has been proposed (83), and preparatory spectroscopic studies are underway (84). Besides the atomic beam techniques described earlier, new experimental approaches based on trapped atoms or ions are also being explored (85, 86).

Perhaps the ‘holy grail’ of this field is the study of atomic PV in radioactive francium isotopes ($Z=87$), the heaviest alkali atomic system, recently reviewed in Reference (87). Both the spin independent and anapole PV contributions are expected to be roughly an order of magnitude larger for Fr (depending on the isotope) than for Cs. In addition, Fr has a large number of isotopes spanning almost 30 neutrons with lifetimes greater than 1 s that cover a wide range of nuclear structure conditions, which in principle permits an unprecedented systematic study of atomic PV in a simple atomic system. With the longest lived isotope ^{223}Fr having a half life of only 23 minutes, a radioactive beam facility is required for a future program of Fr PV studies. Pioneering atomic spectroscopy studies of a number of trapped Francium isotopes have been carried out at

Stony Brook (88), and a collaboration has recently formed with the goal of establishing a long term francium program at the TRIUMF ISAC radioactive beam facility (89), where an actinide production target is planned and necessary to produce the required quantities of Francium (and other heavy systems that are of interest for fundamental symmetry tests such as proposed EDM measurements in radon).

2.2.5 Parity Violation in Compound Nuclei

In contrast to the extremely small ($\simeq 10^{-7}$) PV asymmetries in the two nucleon system, many-body nuclei have over the years provided many examples of parity violation at a much more significant scale, some of them surprisingly large (see e.g. Reference (9) and references therein). For the handful of cases for which reliable nuclear wavefunctions can be used to interpret the data, there is qualitative agreement with predictions of the meson-exchange model as illustrated in Figure 2, albeit with a significant discrepancy in the scale of the pion coupling as discussed earlier. Since the publication of Reference (9), an extensive and in many ways complementary program of PV measurements in compound nuclei has been carried out, dominated by the work of the TRIPLE collaboration at LANSCE. A review of this field was presented in this journal in 1993 (45) focusing on resonances in ^{238}U and ^{232}Th ; an updated comprehensive review of that and more recent data and analysis is provided in Reference (90).

The TRIPLE collaboration measured longitudinal cross section asymmetries for neutron energies in the eV - keV range on a range of nuclear targets. Mixing of S- and P- wave resonances of the same J leads to large PV effects in some cases, with enhancement factors as large as 10^6 relative to the nucleon-nucleon PV asymmetries, due to the high density of states in the compound nucleus. The measurement of a number of PV asymmetries in the same nucleus is a key feature of this program, which is essential to the interpretation of the results. Using a statistical approach, the collaboration was able to extract results for either the RMS weak mixing matrix element M_J or the weak spreading width $\Gamma_w = 2\pi M_J^2/D_J$ where D_J is the level spacing, based on a total of 75 PV resonances observed in 18 nuclei. Important spectroscopic information (J values) for the resonant states was known in some cases, and modelled in other cases, in order to interpret the results. The weak spreading widths were found to be on the order of 10^{-7} eV and roughly constant with mass number, while typical RMS matrix elements were on the scale of 1 meV.

Theoretical treatments have been developed that led to model predictions of the RMS matrix element based on an effective weak interaction with dominant isovector pion and isoscalar ρ exchange contributions taken from DDH predictions. A recent study by Tomsovic et al. (91) outlines a statistical spectroscopy approach for interpreting the experimental RMS matrix elements based on PV asymmetry data from ^{238}U and $^{104,105,106,108}\text{Pd}$ targets to set limits on the weak meson-nucleon coupling constants. To date, a variety of theoretical approaches have been used to predict RMS matrix elements that are in qualitative agreement with experimental data, based on DDH predictions of the coupling constants, and which seem to favour a small value of h_π^1 consistent with the ^{18}F measurements shown in Figure 2, but a comprehensive program to attempt to analyze all the data and set limits on the weak coupling constants has not yet been attempted.

2.3 The End of the Road

Figures 2 and 7 summarize the present state of our knowledge using the meson-exchange framework. We have at present reasonably clear experimental constraints on four linear combinations of the six weak meson-nucleon couplings from a mixture of few nucleon and finite nuclear experiments, not all of which are in agreement with each other. It is fair to say that the phenomenological implications that one can draw from these results are unclear at best. On the one hand, the $\vec{p}p$ experiments now yield a rather stringent set of constraints on the combinations of the DDH couplings h_ρ^{pp} and h_ω^{pp} that govern the asymmetry over a fairly broad range of energy. As we discuss below, h_ρ^{pp} and h_ω^{pp} essentially parameterize the contributions to A_z from the lowest-order, short-range PV potential in the EFT. To the extent that the energy-dependence of A_z is dominated by that of the strong interaction phase shifts that enter matrix elements of these operators as well as the unpolarized cross section, one need not think of h_ρ^{pp} and h_ω^{pp} as being specific to the DDH meson-exchange framework.

On the other hand, the nuclear PV experiments are largely sensitive to two different combinations of the DDH parameters shown in Figure 2: $h_S^{\text{nuc}} \equiv -(h_\rho^0 + 0.7h_\omega^0)$ and $h_V^{\text{nuc}} \equiv h_\pi^1 - 0.12h_\rho^1 - 0.18h_\omega^1$ (7). In the past, it has been the conventional practice to project the constraints from the A_z measurements onto the $h_{S,V}^{\text{nuc}}$ plane by using the DDH theoretical ranges for the $h_\rho^{1,2}$ and h_ω^1 . Here, however, we choose not to do so since we want to minimize the number of theoretical assumptions used in the extraction of information from experiment. Instead, we treat the nuclear experiments separately from the $\vec{p}p$ measurements. In the ideal situation, the analysis of the nuclear experiments would yield a self-consistent region for the $h_{S,V}^{\text{nuc}}$ – a situation that clearly does not emerge from Figure 2. The primary problem seems to be the inclusion of the ^{133}Cs anapole moment constraint, which finds no region of simultaneous consistency with all the other nuclear PV experiments. To explain this discrepancy, one might naturally re-examine the shell model calculation leading to the cesium band. However, theoretical considerations suggest that a more realistic calculation would lead to an even larger discrepancy (7, 24), while the results of more naive shell model computations (18, 19, 25, 26, 27, 28, 29, 30) lead to a similar result. Evidently, additional insight into the many-body physics of nuclear PV is needed before a consistent phenomenology can be obtained with the meson-exchange framework.

Even if such a consistent picture had emerged from experiment, extraction of fundamental information on the $\Delta S = 0$ HWI would still be problematic. To explain why, we consider the physics embodied by the $h_{S,V}^{\text{nuc}}$. As compared with h_ρ^{pp} and h_ω^{pp} , these effective nuclear couplings correspond to different combinations of the short range EFT operators and long-range π -exchange PV potential than those that enter the $\vec{p}p$ asymmetry. However, the nuclear matrix elements of these operators sample the spatial-dependence of both the operators as well as their action on the nuclear wavefunctions, and we have no simple way of disentangling the two as we do for the $\vec{p}p$ asymmetries.

To illustrate, we first consider the momentum space form of the ρ - and ω -exchange operators appearing in V_{DDH}^{PV} . Each term contains a pseudoscalar of the general form $\vec{\sigma}_i \cdot \vec{p}_j$ – where the subscripts refer to nucleons i or j – times a function of the momentum transfer $q = |\vec{q}|$ generated by the meson propagator in the static limit ($q_0 = 0$) and a

hadronic form factor $F_{\rho, \omega}(q^2)$ arising from the meson-nucleon vertices:

$$V_{V-\text{exchange}}^{\text{PV}} \sim \vec{\sigma}_i \cdot \vec{p}_j F_V(q^2) [1 + q^2/m_V^2]^{-1} . \quad (7)$$

For $q \ll m_V$ we may expand in powers of q^2/m_V^2 :

$$V_{V-\text{exchange}}^{\text{PV}} \sim \vec{\sigma}_i \cdot \vec{p}_j F_V(0) \left(1 + \frac{q^2}{m_V^2} [m_V^2 F'(0) - 1] + \dots \right) , \quad (8)$$

where the $+\dots$ indicate higher order terms. In a model-independent approach, the coefficient $[m_V^2 F'(0) - 1]$ of the q^2/m_V^2 term in Eq. (8) would be replaced by an a priori unknown coefficient whose value would have to be taken from either experiment or a QCD computation. A similar statement holds for the higher order terms. At each order n in the expansion, one could also include additional pseudoscalar operators having a different structure than $\vec{\sigma}_i \cdot \vec{p}_j (q^2/m_V^2)^n$. In effect, the meson-exchange framework imposes model-dependent relations between all of the higher-order operator coefficients and those of the lowest order terms – relations that may or may not hold in the SM.

The impact of the higher-order operators on nuclear matrix elements depends on both the values of the operator coefficients as well as the spatial dependence of the nuclear wavefunctions. Extraction of the $h_{S,V}^{\text{mc}}$ from experimental observables relies on *both* the relationships between these operators implicitly assumed by the meson-exchange model as well as on nuclear model-space truncations and other nuclear structure inputs that affect the wavefunctions employed. At present, we have no rigorous way to disentangle the impact of either on the extracted PV couplings, and the constraints in Figure 2 may reflect both artifacts of nuclear structure calculations as well as assumed operator relations. If one seeks to study the fundamental $\Delta S = 0$ HWI experimentally, then one would like to avoid such an implicit reliance on model-dependent assumptions and nuclear structure inputs. The theoretically cleanest way to do so is to exploit effective field theory – wherein operator relations are determined systematically from experiment – and by studying hadronic PV in few-body systems, for which ab initio theoretical computations are available.

3 Effective Field Theory Framework

Effective field theories are ideally suited to situations where there exists a distinct hierarchy of scales. In the present instance, several scales are relevant: the weak scale $v = (\sqrt{2}G_F)^{1/2} = 246$ GeV; the hadronic scale $\Lambda_{\text{HAD}} \approx 1$ GeV; the pion mass and decay constant, $m_\pi \approx 140$ MeV and $F_\pi = 93.2$ MeV, respectively; and the typical momentum Q relevant to a parity-violating hadronic or nuclear process. The distance at which the repulsive core of the strong NN potential becomes dominant, $r \lesssim 0.4$ fm corresponds to a mass scale $\gtrsim 500$ MeV which, for our purposes, we take to be of order Λ_{HAD} . The size of hadronic matrix elements relevant to the HWI is governed by the ratio of F_π^2 to v^2 that is typically normalized to the quantity g_π as in Eq. (4).

The remaining scales can be used to construct an effective Lagrangian out of nucleon and pion fields, where the operators are organized according to powers of Q/Λ . For

processes in which $Q \ll m_\pi$, one should take $\Lambda = m_\pi$, treating the pions as heavy and “integrating them out” of the effective theory. For $Q \gtrsim m_\pi$, the pion must be kept as an explicit degree of freedom, and one should take $\Lambda = \Lambda_{\text{HAD}}$. Consequently, we consider two versions of the EFT corresponding to these two different regimes for Q .

3.1 The Pionless Effective Field Theory

In the PV EFT without pions, the lowest-order pseudoscalar operators contain four nucleon fields and are $\mathcal{O}(Q)$, since they must transform as $\vec{\sigma}_i \cdot \vec{p}_j$. At this order, there nominally exist ten different contact operators. As shown in Reference (8), the most general short-range (“SR”) potential has the coordinate-space form

$$\begin{aligned}
V_{1, \text{SR}}^{\text{PV}}(\vec{r}) = & \frac{2}{\Lambda^3} \left\{ \left[C_1 + (C_2 + C_4) \left(\frac{\tau_1 + \tau_2}{2} \right)_3 + C_3 \tau_1 \cdot \tau_2 + \mathcal{I}_{ab} C_5 \tau_1^a \tau_2^b \right] \right. \\
& (\vec{\sigma}_1 - \vec{\sigma}_2) \cdot \{-i\vec{\nabla}, f_m(r)\} \\
& + \left[\tilde{C}_1 + (\tilde{C}_2 + \tilde{C}_4) \left(\frac{\tau_1 + \tau_2}{2} \right)_3 + \tilde{C}_3 \tau_1 \cdot \tau_2 + \mathcal{I}_{ab} \tilde{C}_5 \tau_1^a \tau_2^b \right] \\
& i(\vec{\sigma}_1 \times \vec{\sigma}_2) \cdot [-i\vec{\nabla}, f_m(r)] \\
& + (C_2 - C_4) \left(\frac{\tau_1 - \tau_2}{2} \right)_3 (\vec{\sigma}_1 + \vec{\sigma}_2) \cdot \{-i\vec{\nabla}, f_m(r)\} \\
& \left. + C_6 i \epsilon^{ab3} \tau_1^a \tau_2^b (\vec{\sigma}_1 + \vec{\sigma}_2) \cdot [-i\vec{\nabla}, f_m(r)] \right\} \quad (9)
\end{aligned}$$

where $\mathcal{I}_{ab} = \text{diag}(1, 1, 2)$ and where the subscript “1” on $V_{1, \text{SR}}^{\text{PV}}(\vec{r})$ essentially indicates that this potential appears at $\mathcal{O}(Q^1)$ in the EFT. In arriving at Eq. (9) we have introduced the function $f_m(\vec{r})$ that is strongly peaked about $r = 0$ with some width $\sim 1/m$ and goes to $\delta^{(3)}(\vec{r})$ in the zero-width ($m \rightarrow \infty$) limit. For practical purposes, we will take $1/m \lesssim 0.4$ fm.

At first glance, one sees a dependence on ten a priori unknown constants C_{1-6} and \tilde{C}_{1-5} that encode information about the short-distance weak interaction between two nucleons⁴. When considering processes with $Q \ll m_\pi$, however, not all of the operators in Eq. (9) are independent. In this regime, PV observables are dominated by mixing between S- and P-waves, for which there exist only five independent spin-isospin amplitudes:

- i) $d_t(k)$, representing ${}^3S_1(I=0) - {}^1P_1(I=0)$ mixing
- ii) $d_s^{0,1,2}(k)$, representing ${}^1S_0(I=1) - {}^3P_0(I=1)$ mixing generated by $I=0, 1, 2$ operators respectively; and
- iii) $c_t(k)$, representing ${}^3S_1(I=0) - {}^3P_1(I=1)$ mixing

where we have used the notation of Danilov (92) and Desplanques and Missimer (10, 93). At the low energies relevant to the pionless EFT, the energy dependence of these

⁴The combination $\tilde{C}_2 - \tilde{C}_4$ does not appear, so that only ten combinations of the eleven constants C_{1-6} and \tilde{C}_{1-5} appear in Eq. (9).

amplitudes is dominated by the strong interaction phase shifts. Denoting the spin singlet and spin triplet strong interaction S-wave scattering amplitudes as $m_s(k)$ and $m_t(k)$, respectively, we have

$$\begin{aligned} d_t(k) &= \lambda_t m_t(k) + \dots \\ d_s^i(k) &= \lambda_s^i m_s(k) + \dots \\ c_t(k) &= \rho_t m_t(k) + \dots \end{aligned} \quad (10)$$

where the $+\dots$ indicate small corrections to the energy dependence arising from the strong P-wave phase shifts. In his early formulation of the problem, Danilov (92) argued for the forms in Eq. (10), omitting the small corrections indicated. In the EFT framework, it is straightforward to derive the proportionality of the S-P amplitudes and the $m_i(k)$ by computing the relevant T-matrix elements and summing up the strong rescattering contributions. In doing so, one finds that at low energies where P-wave rescattering contributions are small, the λ_i and ρ_t are given by the ratio of the lowest order S-P scattering amplitude to the lowest order, parity-conserving S-wave amplitude in a given spin-isospin channel (8).

The coefficients λ_t , λ_s^i , and ρ_t are themselves proportional to various combinations of the C_i and \tilde{C}_i appearing in $V_{1,SR}^{PV}(\vec{r})$. In the zero-range ($m \rightarrow \infty$) limit, one has ⁵ (8)

$$\begin{aligned} \lambda_t &\propto (C_1 - 3C_3) - (\tilde{C}_1 - 3\tilde{C}_3) \\ \lambda_s^0 &\propto (C_1 + C_3) + (\tilde{C}_1 + \tilde{C}_3) \\ \lambda_s^1 &\propto (C_2 + C_4) + (\tilde{C}_2 + \tilde{C}_4) \\ \lambda_s^2 &\propto -\sqrt{8/3}(C_5 + \tilde{C}_5) \\ \rho_t &\propto \frac{1}{2}(C_2 - C_4) + C_6 \quad . \end{aligned} \quad (11)$$

In effect, at low energies, five of the operators in Eq. (9) become redundant, leaving only five independent S-P amplitudes.

Inclusion of finite-range effects leads to modifications of these relations. Arriving at exact relations using state-of-the-art NN potentials remains an unfinished task for many-body theorists. However, we provide approximate expressions by drawing on the work of Desplanques and Benayoun (94). We obtain

$$\begin{aligned} m_N \rho_t &= -\frac{2}{\Lambda^3} \left[B_2 \left(\frac{1}{2}C_2 - \frac{1}{2}C_4 + C_6 \right) + B_3 \left(\frac{1}{2}C_2 - \frac{1}{2}C_4 - C_6 \right) \right] \\ m_N \lambda_t &= -\frac{2}{\Lambda^3} \left[B_4 (C_1 - 3C_3 + \tilde{C}_1 - 3\tilde{C}_3) + B_5 (C_1 - 3C_3 - \tilde{C}_1 + 3\tilde{C}_3) \right] \\ m_N \lambda_s^0 &= -\frac{2}{\Lambda^3} \left[B_6 (C_1 + C_3 + \tilde{C}_1 + \tilde{C}_3) + B_7 (C_1 + C_3 - \tilde{C}_1 - \tilde{C}_3) \right] \\ m_N \lambda_s^1 &= -\frac{2}{\Lambda^3} \left[B_6 (C_2 + C_4 + \tilde{C}_2 + \tilde{C}_4) + B_7 (C_2 + C_4 - \tilde{C}_2 - \tilde{C}_4) \right] \\ m_N \lambda_s^2 &= \frac{4\sqrt{6}}{\Lambda^3} \left[B_6 (C_5 + \tilde{C}_5) + B_7 (C_5 - \tilde{C}_5) \right] \end{aligned} \quad (12)$$

⁵The last equation of Eqs. (46) in Reference (8) contains an error. The sign in front of C_6 should be “+” rather than “-”.

where $\bar{\Lambda} = m_N m_\rho^2 / \Lambda^3$ and where the B_k are linear combinations of the β_{ij}^\pm of Reference (94). For example, using the values of those constants obtained with the Reid Soft Core (RSC) potential, we obtain $B_k = (-0.0043, 0.0005, -0.0009, -0.0022, -0.0067, 0.0003)$ for $k = 2, \dots, 7$, respectively⁶.

The coefficients $B_{2,5,6}$ multiply the combinations of C_i and \tilde{C}_i that one expects to arise in the lowest order EFT [Eq. (11)]. The remaining terms are generated by finite-range contributions that occur beyond leading order. Although we have not included the full set of PV operators and amplitudes that occur at next-to-leading order (NLO), the magnitudes of the $B_{3,4,7}$ – relative to the $B_{2,5,6}$ – give an indication of the magnitude of higher-order effects and of the error associated with working to lowest order. The RSC values obtained in Reference (94) give $|B_3/B_2| = 0.12$, $|B_4/B_5| = 0.41$, and $|B_7/B_6| = 0.04$, suggesting that the impact of neglected higher-order contributions are generally small except in the case of λ_t .

Before considering the application of this framework to specific observables, it is useful to obtain theoretical predictions for the quantities ρ_t and $\lambda_{s,t}$. To that end, we first consider the correspondence with the DDH meson-exchange model and delineate the relationship between the C_i and \tilde{C}_i and the DDH parameters. Using

$$f_m(\vec{r}) = \frac{m^2}{4\pi r} \exp(-mr) \quad (13)$$

with m being the parameter that defines the range of the PV potential, and letting

$$\bar{\Lambda}_V^3 \equiv \frac{\Lambda^3}{m_N m_M^2} \quad (14)$$

for $M = \rho, \omega$ we have⁷

$$\begin{aligned} C_1^{DDH} &= -\frac{1}{2} \bar{\Lambda}_\omega^3 g_\omega h_\omega^0 & C_2^{DDH} &= -\frac{1}{2} \bar{\Lambda}_\omega^3 g_\omega h_\omega^1 \\ C_3^{DDH} &= -\frac{1}{2} \bar{\Lambda}_\rho^3 g_\rho h_\rho^0 & C_4^{DDH} &= -\frac{1}{2} \bar{\Lambda}_\rho^3 g_\rho h_\rho^1 \\ C_5^{DDH} &= \frac{1}{4\sqrt{6}} \bar{\Lambda}_\rho^3 g_\rho h_\rho^2 & C_6^{DDH} &= -\frac{1}{2} \bar{\Lambda}_\rho g_\rho h_\rho^1 \end{aligned} \quad (15)$$

and

$$\begin{aligned} \frac{\tilde{C}_i^{DDH}}{C_i^{DDH}} &= 1 + \chi_\omega \quad i = 1, 2, \\ \frac{\tilde{C}_i^{DDH}}{C_i^{DDH}} &= 1 + \chi_\rho \quad i = 3 - 5 \quad . \end{aligned} \quad (16)$$

⁶We emphasize that the expressions in Eq. (12) are applicable to the EFT without pions. For a discussion of the modifications due to inclusion of explicit pions, see Sec. 3.2 below. In particular, the lowest-order contribution from single pion exchange appears in ρ_t .

⁷The corresponding expressions given in Eq. (14) of Reference (8) contain typographical errors. The quantity Λ_V should contain only two powers of m_M in the denominator and each of the C_i should be proportional to the product of a strong coupling g_M and the relevant h_M^i as in Eqs. (14-16) here.

Using Eqs. (15,16) one can easily obtain the expressions for ρ_t , λ_t , and $\lambda_s^{0,1,2}$ and employ the DDH best values and reasonable ranges for the PV meson-nucleon couplings to obtain the predictions for the PV LECs listed in Table 2. The results in columns 2-4 were obtained by retaining only the combinations of the C_i , \tilde{C}_i that arise at lowest order in the EFT. Column five contains estimates of the size of higher-order contributions, based on the DDH best values for the C_i , \tilde{C}_i and the terms in Eqs. (12) proportional to $B_{3,4,7}$.

To obtain a sense of the possible variations in theoretical predictions for the PV LECs from their correspondence with the DDH parameterization, we consider two approaches. First, we vary the values of the strong couplings in Eqs. (15) in accordance with the Bonn one pion exchange potential as suggested by Miller (95). As indicated in Table 2, doing so changes both the overall magnitude of the C_i and \tilde{C}_i as well as the relation between the two and leads to generally wider ranges for the PV LECs than obtained with the values of the strong couplings originally used by DDH. Second, we give expectations using naive dimensional analysis (NDA) considerations, as discussed in Section 3.2 below. The NDA arguments suggest that the magnitudes of the C_i and \tilde{C}_i ought to be of order $16\pi^2 \sim 150$, but do not fix the signs of the C_i and \tilde{C}_i . To translate the NDA estimates into predictions for the five LECs, we simply take the magnitudes of the combinations of C_i and \tilde{C}_i appearing in Eqs. (12) to be the NDA expectation for any one of them.

Table 2: *Predictions for the five, PV low energy constants (LECs) characterizing hadronic PV in the pionless EFT. All values are quoted in units of $g_\pi = 3.8 \times 10^{-8}$. Estimates are obtained using Reid Soft Core potential as in Reference (94) ; DDH values are taken from Reference (6)*

PV LEC	DDH Best	DDH range	DDH plus Bonn	higher order	NDA
$m_N \rho_t$	0.05	0.07 \rightarrow 0.03	0.18 \rightarrow 0.08	± 0.006	± 0.38
$m_N \lambda_t$	0.84	-1.00 \rightarrow 2.48	-2.44 \rightarrow 6.12	± 1.2	± 0.31
$m_n \lambda_s^0$	3.82	-4.86 \rightarrow 11.7	-9.84 \rightarrow 22.96	± 0.09	± 0.64
$m_N \lambda_s^1$	0.37	0.64 \rightarrow 0.21	1.53 \rightarrow 0.54	± 0.0006	± 0.64
$m_N \lambda_s^2$	2.72	2.17 \rightarrow 3.15	3.83 \rightarrow 5.55	± 0.06	± 3

We note that in obtaining the correspondence between the PV LECs and the DDH predictions in the meson-exchange model, we have not included contributions from the parameter $h_\rho^{1'}$ that appears in $V_{\text{DDH}}^{\text{PV}}$. Using the estimate of Reference (14) for this parameter would increase the magnitude of ρ_t appearing in Table 2, though not substantially. Generally, analyses of hadronic PV using the meson-exchange model have neglected this parameter since its contribution to $V_{\text{DDH}}^{\text{PV}}$ has the same spin-isospin structure as for the π exchange contribution but is suppressed by its short range. In the EFT framework, this term corresponds to the operator proportional to C_6 that – along with $C_{2,4}$ – contributes to ρ_t . Since the coefficients of $C_{2,4,6}$ in ρ_t have comparable magnitude, we see no model-independent reason to neglect the C_6 contribution in the most general analysis.

With the foregoing set of benchmarks in hand, it is instructive to consider the dependence of various few-body PV observables on the λ_i and ρ_t and to outline a program

of high precision measurements that could be used to determine these parameters. The few-body PV observables of interest include:

- Polarized $\vec{p}p$ scattering at 13.6 and 45 MeV, yielding the asymmetry A_z^{pp} ,
- Polarized $\vec{p}\alpha$ scattering at 46 MeV, giving $A_z^{p\alpha}$,
- Radiative $\vec{n}p$ capture at low energy: $\vec{n}p \rightarrow d\gamma$, yielding the photon asymmetry A_γ^d ,
- Radiative np capture with unpolarized neutrons, giving the photon circular polarization P_γ^d , or alternatively, the asymmetry A_L^γ in $\vec{\gamma}d \rightarrow np$,
- Rotation through an angle ϕ about the momentum direction of polarized neutron spin passing through ${}^4\text{He}$, from which one extracts the quantity $d\phi^{n\alpha}/dz$,
- Radiative capture of polarized neutrons on deuterium at threshold, $\vec{n}d \rightarrow t\gamma$, yielding the photon asymmetry A_γ^t .

Explicit expressions for these quantities in terms of the S-P amplitude parameters have been given in references (10, 93) and elsewhere. In Table 3, we give the coefficients of the five PV LECs as they appear in various observables. Theoretical expectations for these observables in the pionless EFT can be obtained using Tables 2 and 3. We emphasize that these expectations will, in general, differ when going to the EFT with explicit pions discussed in Section 3.2. In particular, the parameter $m_N\rho_t$ that governs the asymmetry A_γ^d will be dominated by LO pion exchange, assuming h_π^1 has its natural size. In Table 3 we also show the most precise experimental results that have been published to date for these observables. Notably, only A_z^{pp} and $A_z^{p\alpha}$ have been measured to sufficient precision to establish a nonzero PV effect that can be used to constrain the PV LECs. A review of recent, ongoing and prospective efforts to obtain precision measurements of these important few-body PV effects appears in Section 3.4 below.⁸

It should be remarked that the longitudinal asymmetry A_z^{pd} in $\vec{p}d$ scattering was measured to high precision at 43 MeV (98, 99) in the 1980's, but remains to be analyzed in a theoretical framework accounting for PV in both elastic scattering and breakup channels, both of which contributed to the experimental signal. There exist also several additional possibilities for few-body experiments, for which we have not yet obtained expressions for the PV observables in terms of the PV LECs. These include measurements of PV neutron spin rotation on hydrogen, $d\phi^{np}/dz$ and deuterium, $d\phi^{nd}/dz$, and one could also consider the circular polarization P_γ^t in $nd \rightarrow t\gamma$ as well as perhaps even the transmission asymmetry of unpolarized neutrons through polarized ${}^3\text{He}$. With realistic prospects for performing some or all of these measurements in the future, deriving the appropriate expressions would clearly be important.

⁸The measurement of P_γ^d is particularly challenging because of the limited sensitivity of conventional γ ray circular polarimeters in the \sim MeV energy range; an alternative measurement of A_L^γ close to threshold yields the same physics and may be more accessible to experiment. A possible experiment is at the early stages of development in Athens (70), as mentioned in Section 2.2, but is not discussed further in Section 3.4.

Table 3: *Sensitivities of selected PV observables to the five PV LECs. The first column gives the observable, while subsequent columns give the coefficients of a given PV LEC. For the pp asymmetry, k is the incident proton momentum in the lab frame. The final columns give the most precise experimental limits to date and their references; for the pp case, we quote the 13.6 and 45 MeV measurements, to which the lowest order EFT best applies. Note that the $p\alpha$ asymmetry is evaluated at 46 MeV; $d\phi^{n\alpha}/dz$ is evaluated in rad/m.*

Observable	$m_N\rho_t$	$m_n\lambda_t$	$m_N\lambda_s^0$	$m_N\lambda_s^1$	$m_N\lambda_s^2/\sqrt{6}$	Expt. (10^{-7})	Ref.
$A_z^{pp}(k)$	0	0	$4k/m_N$	$4k/m_N$	$4k/m_N$	-0.93 ± 0.21 -1.50 ± 0.22	(52) (53)
$A_z^{p\alpha}$	-1.07	-0.54	-0.72	-0.48	0	-3.3 ± 0.9	(96)
P_γ	0	0.63	-0.16	0	0.32	1.8 ± 1.8	(63)
A_γ^d	-0.107	0	0	0	0	0.6 ± 2.1	(65)
$d\phi^{n\alpha}/dz$	-2.68	1.34	1.8	-1.2	0	8 ± 14	(76)
A_γ^t	-3.56	-1.39	-0.95	-0.24	1.18	42 ± 38	(97)

Limits of the pionless EFT

Before discussing the EFT with pions, it is instructive to investigate the limits of validity of the pionless theory by considering the the low-energy $\vec{p}\vec{p}$ asymmetry as an illustrative example. Again, considering only S-P mixing, it is straightforward to show that (8):

$$A_z^{pp} = \frac{\sigma_+ - \sigma_-}{\sigma_+ + \sigma_-} = \frac{4k \operatorname{Re}[m_s^*(k)d_s^{pp}(k)]}{|m_s(k)|^2} \simeq 4k\lambda_s^{pp} \quad . \quad (17)$$

where where we have neglected small corrections arising from the P-wave phase shifts as before. A more complete decomposition of A_z^{pp} in terms of higher partial waves was first worked out by Simonius (46) and subsequently studied by several authors. A recent analysis using state-of-the-art NN potentials was performed in Reference (54) and used to extract the DDH parameters h_ρ^{pp} and h_ω^{pp} .

Following Simonius' original formulation, one may write the asymmetry as

$$A_z^{pp} = \sum_{\text{even } J} f_{J\pm}(E)K_{J\pm}(E, \theta) \quad , \quad (18)$$

where the “ \pm ” indicate the orbital angular momentum $L = J \pm 1$ and where E and θ are the energy and scattering angle, respectively. The $f_{J\pm}$ are “reduced” PV transition amplitudes and the $K_{J\pm}$ contain all the dependence on the strong phases that arise from

rescattering. For the $J = 0$ partial wave, only f_{0+} exists, and it is proportional to the combination d_s^{pp} of the S-P amplitudes d_s^i that enter the $\vec{p}\vec{p}$ process:

$$d_s^{pp} = -2if_{0+} \exp i [\delta(^1S_0) + \delta(^3P_0)] \quad . \quad (19)$$

To the extent that one may neglect the finite (but short) range of the PV potential, d_s^{pp} and f_{0+} are proportional to λ_s^{pp} . Moreover, in obtaining Eq. (17), we have neglected the dependence of d_s^{pp} on $\delta(^3P_0)$. Doing so is equivalent to taking $K(E, \theta) \propto k$.

While this approximation holds to a high degree for accuracy for low energy interactions, it breaks down for $E \sim 100$ MeV ($k \sim 300$ MeV). Due to cancellations between the effects of the S- and P-wave phase shifts in d_s^{pp} that occur above this energy, the contribution of the $J = 0$ partial wave to A_z^{pp} falls rapidly, going to zero at $E = 227$ MeV. Moreover, the contribution from the $J = 2$ partial wave – dominated by the 1D_2 – 3P_2 (f_{2-}) mixing – becomes appreciable. Taking advantage of the former, the beam energy for the TRIUMF A_z^{pp} (221 MeV) measurement was optimized, accounting for finite acceptance of the apparatus, to ensure that the f_{0+} contribution was entirely cancelled, so that the asymmetry was determined almost entirely by the f_{2-} contribution (47, 54). Thus, a combined analysis of the TRIUMF and lower-energy A_z^{pp} measurements yields constraints on the two amplitudes f_{0+} and f_{2-} . In effect, one may treat the values of h_ρ^{pp} and h_ω^{pp} obtained in Reference (54) as equivalent parameterizations of these two partial wave transition amplitudes and need not tie them specifically to the meson-exchange framework.

Clearly, at the energies of the recent TRIUMF experiment, the lowest-order EFT is no longer applicable, and one must include $\mathcal{O}(Q^3)$ operators in V_{SM}^{PV} that characterize P-D mixing. Doing so introduces a host of new, a priori unknown operator coefficients. At the same time, the redundancy of operators in the $\mathcal{O}(Q)$ V_{SR}^{PV} in Eq. (9) that holds for the S-P amplitudes breaks down, and all ten lowest order operators become independent. Determining all of these constants from experiment would be unrealistic, so we will restrict our attention to the energy range where the lowest order EFT applies.

3.2 PV EFT with Pions

For PV processes involving few-body nuclei, the relevant energy scale Q is no longer set solely by experimental kinematics, but also includes the relevant internal momentum of the bound nucleons. Since the latter can be as large as the Fermi momentum of $\gtrsim 200$ MeV, it is no longer reasonable to treat the pion as heavy. For decades, phenomenological strong interaction potentials for light nuclei have included a long-range π -exchange component. In the case of the EFT formulation, treating pionic contributions consistently has presented challenges. The difficulty arises from the presence of two-nucleon poles in iterated π -exchange amplitudes whose contributions are enhanced by $\sim m_N/Q$ relative to naive expectations. These enhanced contributions spoil the “power counting” in Q/Λ that is essential to the success of the EFT approach. Thus, one must sum strong pion exchange to all orders in order to obtain a consistent treatment. Indeed, as shown in Reference (100), treating the pion perturbatively as in the framework of references (101, 102) does not lead to a convergent expansion in all channels of the NN interaction.

An alternate formulation, originally proposed by Weinberg (103, 104), entails performing the all-orders resummation in terms of the effective strong potential. In order to be self-consistent, however, it appears that one must simultaneously perform the EFT expansion of the potential about the chiral limit (105, 106, 107): $m_\pi = 0$, since a full resummation of the chiral symmetry-breaking component of the one pion-exchange (OPE) potential leads to inconsistent renormalization (101, 102, 105, 106, 107). Although the chiral expansion treatment of the Weinberg approach is still under development, we follow Reference (8) and employ it here.

The basis for the EFT with pions is chiral perturbation theory (χ PT) whose formalism is well-known and will not be repeated here. However, we note that its formulation for hadronic PV processes was first written down by Kaplan and Savage (108), whose notation follow. The non-linear dependence of the effective Lagrangian on the pion is implemented via the field

$$\xi = \exp\left(\frac{i\pi^a\tau^a}{2F_\pi}\right), \quad (20)$$

where π^a , $a = 1, 2, 3$ are the isospin components of the pion field. Defining the quantity

$$X_-^3 = \xi^\dagger\tau^3\xi - \xi\tau^3\xi^\dagger, \quad (21)$$

the lowest-order Lagrangian for a PV interaction of the pion with a single nucleon is

$$\begin{aligned} \mathcal{L}_{\pi N, PV}^{(-1)} &= -\frac{h_\pi^1}{2\sqrt{2}}\bar{N}X_-^3N \\ &= -ih_\pi^1(\bar{p}n\pi^+ - \bar{n}p\pi^-) + \dots \end{aligned} \quad (22)$$

where the “ $+\dots$ ” indicate the higher order terms in odd powers of $(\pi^a\tau^a/F_\pi)$ that arise from expanding the exponential in ξ . The leading term in the Lagrangian in Eq. (22) is identical to the PV Yukawa interaction in the DDH model. Consequently, its contribution to the PV NN potential will be the same as the first term in Eq. (2):

$$V_{(-1, \text{LR})}^{\text{PV}}(\vec{r}) = i\frac{h_\pi^1 g_A m_N}{\sqrt{2}F_\pi} \left(\frac{\vec{\tau}_1 \times \vec{\tau}_2}{2}\right)_3 (\vec{\sigma}_1 + \vec{\sigma}_2) \cdot \left[\frac{\vec{p}_1 - \vec{p}_2}{2m_N}, w_\pi(r)\right] \quad (23)$$

The “ -1 ” subscript indicates that this long-range (“LR”) potential is $\mathcal{O}(Q^{-1})$, a feature most readily seen from its momentum-space form:

$$V_{(-1, \text{LR})}^{\text{PV}}(\vec{q}) = -i\frac{g_A h_\pi^1}{\sqrt{2}F_\pi} \left(\frac{\vec{\tau}_1 \times \vec{\tau}_2}{2}\right)_3 \frac{(\vec{\sigma}_1 + \vec{\sigma}_2) \cdot \vec{q}}{q^2 + m_\pi^2}, \quad (24)$$

where $\vec{q} = \vec{p}_1 - \vec{p}_1' = \vec{p}_2' - \vec{p}_2$ is the three-momentum of the exchanged pion, \vec{p}_i (\vec{p}_i') is the initial (final) momentum of nucleon i , and $q = |\vec{q}|$.

Since the PV potential must transform as a pseudoscalar, the operators in it will contain odd numbers of derivatives. Thus, one would expect the sub-leading terms to be $\mathcal{O}(Q)$, as in $V_{(1, \text{SR})}^{\text{PV}}$. In principle, loop corrections to the Lagrangian (22) or to $V_{(-1, \text{LR})}^{\text{PV}}(\vec{r})$ could bring in a factor of m_π or p^2/m_π , leading to an $\mathcal{O}(Q^0)$ component. Explicit computations, however, indicate that no such contributions exist. Consequently, the subleading components of the potential start off at $\mathcal{O}(Q)$ (next-to-next-to-leading order, NNLO), and it is convenient to distinguish them according to their range:

- i) **Short range:** $V_{(1, \text{SR})}^{\text{PV}}$ as in Eq. (9) but with $\Lambda = \Lambda_{\text{HAD}} \approx \Lambda_\chi = 4\pi F_\pi$.
- ii) **Medium range:** $V_{(1, \text{MR})}^{\text{PV}}$, generated by the two pion-exchange diagrams of Figure 1c) and proportional to h_π^1 . The structure of the operator is most conveniently given in momentum space, as it carries a non-analytic dependence on pion momentum and mass (8):

$$V_{(1, \text{MR})}^{\text{PV}}(\vec{q}) = -\frac{1}{\Lambda_\chi^3} \left\{ \tilde{C}_2^{2\pi}(q) \frac{\tau_1^z + \tau_2^z}{2} i (\vec{\sigma}_1 \times \vec{\sigma}_2) \cdot \vec{q} + C_6^{2\pi}(q) i \epsilon^{ab3} [\vec{\tau}_1 \times \vec{\tau}_2]_3 (\vec{\sigma}_1 + \vec{\sigma}_2) \cdot \vec{q} \right\}, \quad (25)$$

where

$$\begin{aligned} \tilde{C}_2^{2\pi}(q) &= 4\sqrt{2}\pi g_A^3 h_\pi^1 L(q) \\ C_6^{2\pi}(q) &= -\sqrt{2}\pi g_A h_\pi^1 L(q) + \frac{3\sqrt{2}}{2}\pi [3L(q) - H(q)] g_A^3 h_\pi^1, \end{aligned} \quad (26)$$

and

$$\begin{aligned} L(q) &= \frac{\sqrt{4m_\pi^2 + q^2}}{q} \ln \left(\frac{\sqrt{4m_\pi^2 + q^2} + q}{2m_\pi} \right), \\ H(q) &= \frac{4m_\pi^2}{4m_\pi^2 + q^2} L(q). \end{aligned} \quad (27)$$

- iii) **Long range:** $V_{(1, \text{LR})}^{\text{PV}}$, generated by one-loop corrections to the PV πNN Yukawa and parity conserving strong vertices as well as by additional operators having a distinct structure from the lowest order potential. As discussed in Reference (8), the impact of all but one of the NNLO PV operators can be absorbed in to $V_{(-1, \text{LR})}^{\text{PV}}$ and $V_{(1, \text{SR})}^{\text{PV}}$ through a suitable redefinition of the operator coefficients. The remaining PV operator and PC operators give rise to the momentum space potential (8)

$$\begin{aligned} V_{1, \text{LR}}^{\text{PV}}(\vec{p}_1, \dots, \vec{p}_2') &= \frac{g_A k_\pi^{1a}}{\Lambda_\chi F_\pi^2} \left(\frac{\vec{\tau}_1 \times \vec{\tau}_2}{2} \right)_3 \left[\frac{\vec{\sigma}_1 \cdot \vec{p}_1' \times \vec{p}_1 \vec{\sigma}_2 \cdot \vec{q}_1}{q^2 + m_\pi^2} + (1 \leftrightarrow 2) \right] \\ &+ i \frac{g_A h_\pi^1}{\sqrt{2} m_N^2 F_\pi} \left(\frac{\vec{\tau}_1 \times \vec{\tau}_2}{2} \right)_3 \frac{1}{q^2 + m_\pi^2} \left\{ \right. \\ &\frac{1}{4} [(|\vec{p}_1|^2 - |\vec{p}_1'|^2) \vec{\sigma}_1 \cdot (\vec{p}_1' + \vec{p}_1) - (1 \leftrightarrow 2)] \\ &- \frac{1}{8} [(|\vec{p}_1|^2 + |\vec{p}_1'|^2) \vec{\sigma}_1 \cdot \vec{q} + (1 \leftrightarrow 2)] \\ &\left. + \frac{1}{4} [\vec{\sigma}_1 \cdot \vec{p}_1' \vec{q} \cdot \vec{p}_1 + \vec{\sigma}_1 \cdot \vec{p}_1 \vec{q} \cdot \vec{p}_1' + (1 \leftrightarrow 2)] \right\} \end{aligned} \quad (28)$$

where $\vec{q}_i = \vec{p}_i' - \vec{p}_i$ and k_π^{1a} is a constant that must be determined from experiment.

In addition to considering the potential through $\mathcal{O}(Q)$, one must also include two-body current operators that contribute to the same order when considering PV processes

involving photons. These operators include the standard PV meson-exchange currents associated with the π -exchange potential and those arising from the covariant derivatives in $V_{(1, \text{SR})}^{\text{PV}}$. In addition, there exists a new, independent current operator (8)

$$\vec{J}(\vec{x}_1, \vec{x}_2, \vec{q}) = \frac{\sqrt{2}g_A\bar{C}_\pi m_\pi^2}{\Lambda^2 F_\pi} e^{-i\vec{q}\cdot\vec{x}_1} \tau_1^+ \tau_2^- \vec{\sigma}_1 \times \vec{q} \vec{\sigma}_2 \cdot \hat{r} H_\pi(r) + (1 \leftrightarrow 2), \quad (29)$$

where

$$H_\pi(r) = \frac{\exp(-m_\pi r)}{m_\pi r} \left(1 + \frac{1}{m_\pi r}\right), \quad (30)$$

and \bar{C}_π is an additional LEC parameterizing the leading PV $NN\pi\gamma$ interaction.

PV EFT with pions: new features

In comparison with the DDH meson-exchange potential, the EFT with explicit pions introduces several qualitatively distinct features. First, the $\mathcal{O}(Q)$, long range operators in Eq. (28,29) have no analog in the DDH framework and introduce two new unknown constants, k_π^{1a} and \bar{C}_π . Given the novel nature of these operators, the impact of their contributions to the observables discussed above has yet to be determined with explicit, few-body computations. Based on the isospin structure of these two operators, however, one would expect them to contribute to the same processes, such as $\vec{n}p \rightarrow d\gamma$, that are sensitive to the LO π -exchange potential. Power counting implies that the magnitude of their contribution should be smaller than that of $V_{(-1, \text{LR})}^{\text{PV}}$, but their long range character suggests that they should have a greater impact than the operators in $V_{(1, \text{SR})}^{\text{PV}}$. Future few-body calculations should test these expectations.

The two π -exchange (TPE) medium range potential, $V_{(1, \text{MR})}^{\text{PV}}$, is similarly a new feature of the EFT framework. In the past, others have attempted to introduce PV TPE using model frameworks (see, *e.g.*, Reference (109)), but to our knowledge, the result in Eq. (25) gives the first formulation that is model-independent and consistent with the symmetries of QCD. The operator coefficients $\tilde{C}_2^{2\pi}$ and $C_6^{2\pi}$ have been labelled to indicate their correspondence with the operators in $V_{(1, \text{SR})}^{\text{PV}}$, but as indicated in Eq. (26), the coefficients are fixed in terms of h_π^1 and are not independent free parameters. The operator proportional to $C_6^{2\pi}$ has the same isospin structure as $V_{(-1, \text{LR})}^{\text{PV}}$ and will contribute to any process – such as $\vec{n}p \rightarrow d\gamma$ – that is sensitive to the LO π -exchange potential. The operator proportional to $\tilde{C}_2^{2\pi}$ has the same structure as the $h_\omega^1(1 + \chi_\omega)$ term in the DDH potential and will, therefore, generate a medium range contribution to any observable sensitive to the latter combination in the meson-exchange model. In particular, this operator will contribute to both the f_{0+} and f_{2-} partial wave terms in A_z^{pp} , implying that this observable is sensitive to h_π^1 at the same order in Q as the the short-range effects enter. In either case, proper inclusion of TPE medium range potential will affect the determination of h_π^1 obtained from a global analysis of few-body PV observables.

In principle, one should also take into account three-body PV forces that arise in the EFT with pions, as we will discuss few-body experiments in systems involving three or more nucleons. As discussed in Reference (8), three-body PV forces do not arise at $\mathcal{O}(Q)$, so we restrict our attention to the two-body PV EFT interaction.

PV LECs: naive dimensional analysis

Beyond these qualitative observations, we are not able to make any quantitative statements regarding the relative importance of the new features of the PV EFT with pions. Evaluating their contributions to specific observables now constitutes an open problem for few-body theorists. That being said, it is instructive to estimate the size of the constants C_i , \tilde{C}_i , h_π^1 , k_π^{1a} , and \bar{C}_π that arise in the EFT. A systematic way of doing so – known as “naive dimensional analysis” (NDA) – was developed by Georgi and Manohar (110) and has successfully explained the size of a variety of LECs in χ PT. According to NDA, one should construct operators by scaling fields and derivatives to their natural scales:

$$\left(\frac{D_\mu}{\Lambda_\chi}\right)^d \left(\frac{\pi}{F_\pi}\right)^p \left(\frac{\bar{N}N}{\Lambda_\chi F_\pi^2}\right)^{f/2} \times (\Lambda_\chi F_\pi)^2 \times (g_\pi)^n, \quad (31)$$

where d , p , $f = 2k$, k and n are positive integers and where g_π is as given in Eq. (4). Consequently, one expects the PV LEC’s to have the magnitudes

$$h_\pi^1 \sim \left(\frac{\Lambda_\chi}{F_\pi}\right) g_\pi \sim 10g_\pi \quad (32)$$

$$C_i, \tilde{C}_i \sim \left(\frac{\Lambda_\chi}{F_\pi}\right)^2 g_\pi \sim 100g_\pi \quad (33)$$

$$k_\pi^{1a}, \bar{C}_\pi = g_\pi \sim g_\pi. \quad (34)$$

It is interesting that since $\Lambda_\chi/F_\pi = 4\pi \sim 12$, the NDA estimates for h_π^1 and the C_i , \tilde{C}_i are roughly equal to the expectations based on correspondence with the DDH best values. In contrast, one expects the new long range LECs k_π^{1a} and \bar{C}_π to be an order of magnitude smaller than h_π^1 . This difference, however, simply reflects the conventions used above in normalizing the various operators.

PV EFT: phenomenology

The phenomenology of the PV EFT with pions is clearly more challenging than for the pionless theory, since one encounters additional unknown parameters when working to $\mathcal{O}(Q)$, and since a variety of new contributions remain to be computed. In principle, there exists a viable experimental program that could determine the constants to this order, including the six measurements highlighted in Section 3.1 for the pionless theory plus two additional, independent experiments. As noted in Section 3.1, possibilities for the latter include a careful analysis of the $\vec{p}d$ scattering asymmetry results for A_z^{pd} (98, 99) and future neutron spin rotation measurements on hydrogen or deuterium. Recently, the possibility of performing PV photo- and electro-production experiments on the single nucleon to determine the of πN and γN couplings has received considerable attention. Carrying out these experiments – which we discuss below – would provide additional, independent input for the determination of the PV LECs.

Theoretically, the extraction of these constants from experiment will require new calculations to determine the contributions from (a) the medium-range, TPE potential (25), (b) the NNLO single pion-exchange potential (28), and (c) the meson-exchange

current (29). At present, only the dependence on h_π^1 generated by LO pion-exchange is known:

$$m_N \rho_t = 1.04 h_\pi^1 + m_N \rho_t^{\text{SR}} + m_N \Delta \rho_t, \quad (35)$$

where ρ_t^{SR} gives the dependence of the 3S_1 - 3P_1 mixing on the constants appearing in $V_{1, \text{SR}}^{\text{PV}}$ as in Eq. (12); $\Delta \rho_t$ gives the presently unknown contributions generated by $V_{1, \text{MR}}^{\text{PV}}$ and $V_{1, \text{LR}}^{\text{PV}}$; and the first term on the right side of Eq. (35) is generated by $V_{-1, \text{LR}}^{\text{PV}}$ as computed by Desplanques and Benayoun using the Reid Soft Core potential (94). Since $V_{1, \text{MR}}^{\text{PV}}$ contains spin-isospin structures corresponding to both the C_6 and C_2 terms in $V_{1, \text{SR}}^{\text{PV}}$, the LEC λ_s^1 will also contain a dependence on h_π^1 generated by two-pion exchange. In addition to computing these new contributions to ρ_t and λ_s^1 , theorists must also determine new meson-exchange current contributions to processes such as $\vec{n} + p \rightarrow d + \gamma$, generated associated with $V_{1, \text{MR}}^{\text{PV}}$ and $V_{1, \text{LR}}^{\text{PV}}$ and required by gauge invariance, as well as the contribution from the new current in Eq. (29).

Assuming that a successful program is completed and the complete set of PV LECs through $\mathcal{O}(Q)$ are extracted from experiment, the values of these parameters would provide model-independent benchmarks for Standard Model theory. In this case, the theoretical challenge would be analogous to the one encountered with χPT for pseudoscalar mesons, where for example, at $\mathcal{O}(Q^4)$, there exist ten independent LECs that have been determined from experiment. The theoretical task is now to explain how the dynamics of QCD give rise to the values of these constants, and to that end, a number of approaches have been pursued. Ultimately, of course, one would like to compute these constants using lattice QCD, but given the difficulties in putting two or more hadrons on the lattice, approaches based on symmetry arguments or models are an attractive, interim alternative. A particularly fruitful direction involves taking the limit of QCD with a large number of colors (N_C), wherein one expects the exchange of heavy mesons, such as the ρ and ω , to dominate the underlying QCD dynamics of the LECs. In the $N_C = 3$ world that we inhabit, this large- N_C picture of “resonance saturation” works remarkably well in accounting for the values of the constants. It remains to be understood why large the large N_C limit is so successful in this case, and future lattice QCD computations should address this problem⁹.

In the case of the PV LEC’s, the results from experiment should teach us whether the large N_C resonance saturation picture applies to the $\Delta S = 0$ HWI involving baryons as well as to strong interactions between light mesons. In effect, the DDH model *assumes* the validity of resonance saturation, albeit with a truncated spectrum of exchanged mesons that may or may not reflect accurately the underlying dynamics. As discussed at the outset of this article, there exists ample evidence that QCD symmetry arguments fall short when confronting the phenomenology of the $\Delta S = 1$ HWI, so one should apply caution when adopting another one (viz, large N_C) to predict weak, hadronic $\Delta S = 0$ processes. At the same time, one would like to derive as much model-independent information as possible on the HWI in each sector, so that one can gain new insights into the

⁹At the same time, it has become important to know the values of certain $\mathcal{O}(Q^6)$ constants that presently cannot be taken from experiment and that are needed for the extraction of the Cabibbo-Kobayashi-Maskawa matrix element V_{us} from K_{e3} decay data. The insights and techniques developed to explain the $\mathcal{O}(Q^4)$ constants will be essential in obtaining reliable theoretical values for the unknown higher order terms.

puzzles associated with strangeness-changing processes. For example, if one ultimately found a set of PV LECs that agreed with expectations based on NDA and resonance saturation, one might conclude that the breakdown of symmetry-based expectations in the $\Delta S = 1$ sector is associated with the dynamics of the participating strange quark. On the other hand, should the PV LECs depart substantially from NDA and large N_C expectations, one would look elsewhere to determine dynamics general to all sectors of the HWI.

3.3 Recent Theoretical Work

As the foregoing discussion makes evident, there now exists ample motivation for new theoretical work within the context of the EFT for hadronic PV. The past decade has seen initial efforts in this direction, and we review some of this work here.

Few-Body Systems.

In the two-body sector, recent interest has focused on the asymmetry A_γ^d for $\vec{n}p \rightarrow d\gamma$, where new computations using EFT and Green's function Monte Carlo methods have been used. The lowest order EFT computation yields the asymmetry (111)

$$A_\gamma^d = -\frac{2m_N}{\gamma^2} \frac{\text{Re}[(X + Y)^*W]}{2|X|^2 + |Y|^2} \quad (36)$$

where X and Y give contributions to the parity-conserving $\vec{n}p \rightarrow d\gamma$ amplitude for an initial 3S_1 and 1S_0 state, respectively, and W gives the PV amplitude:

$$W = -g_A h_\pi^1 \frac{\sqrt{\pi}\gamma}{2\pi F_\pi} \left[\frac{m_\pi}{(m_\pi + \gamma)^2} - \frac{m_\pi^2}{2\gamma^3} \ln\left(\frac{2\gamma}{m_\pi} + 1\right) + \frac{m_\pi^2}{\gamma^2(m_\pi + \gamma)} \right], \quad (37)$$

with $\gamma = \sqrt{m_N B}$ and B being the deuteron binding energy¹⁰. From these expressions, one obtains $A_\gamma^d = -0.17h_\pi^1$. The coefficient of h_π^1 in this result is nearly a factor of two larger than in previous, wavefunction-based computations, and stimulated considerable follow-up theoretical activity (41, 42, 67, 112, 114). In particular, the authors of Reference (114) computed the asymmetry to NLO in the Weinberg scheme, using two-body wavefunctions derived from the Argonne v_{18} potential, and obtained $A_\gamma^d = -0.10h_\pi^1$, in close agreement with previous results obtained using Siegert's theorem, $A_\gamma^d \simeq -0.11h_\pi^1$. Subsequently, the authors of Reference (41) performed a wavefunction-based computation in the DDH framework, using Argonne v_{18} , Nijmegen-I, and Bonn-CD wavefunctions and found $A_\gamma^d = -(0.106 \rightarrow 0.109)h_\pi^1 + \dots$, where the range corresponds to the choice of different potentials and where the $+\dots$ indicate small, $\mathcal{O}(10^{-9})$ contributions from the short-range terms in the DDH potential.

From a more academic perspective, several computations of the deuteron anapole moment have been performed using EFT and wavefunction methods (68, 115, 116, 117, 118). The LO EFT result is (115):

$$F_A^{(D)} = -\frac{eg_A h_\pi^1 m_N^2}{24F_\pi} \left[\kappa_1 \frac{m_\pi + \gamma}{(m_\pi + 2\gamma)^2} + \frac{2m_\pi + 9\gamma}{6(m_\pi + 2\gamma)^2} \right] \quad (38)$$

¹⁰In writing down Eq. (37), we used an overall sign that is opposite the one appearing in Reference (111), thereby following the conventions used elsewhere in the literature (112, 113).

where $\kappa_1 \simeq 1.85$ is the isovector anomalous magnetic moment of the deuteron. The numerical value of $F_A^{(D)}$ obtained from this expression has the same sign but a magnitude that is $\sim 40 - 50\%$ larger than results obtained using a wavefunction computation (68) or Weinberg EFT approach (117). From a practical standpoint, the impact of the deuteron anapole moment would be most relevant to the interpretation of PV elastic $\vec{e}d$ scattering, wherein it would generate a potentially important contribution to the isoscalar axial vector response (35). Since the latter vanishes at tree-level in the Standard Model, it is particularly transparent to higher-order effects, such as electroweak radiative corrections, the strange quark axial vector current, and hadronic PV. To date, however, no experiments have been proposed to study the PV elastic deuterium asymmetry.

Single Nucleon Sector.

From the standpoint of theoretical interpretability, PV pion photo- and electroproduction processes involving single nucleon targets offer several advantages. In particular, they provide a means for accessing the PV πNN couplings directly without having to disentangle the short- and medium-range effects discussed above. Moreover, the use of χ PT to describe low-energy pion-nucleon interactions is well established and has been thoroughly studied in the parity conserving sector. Looking to future work in QCD, it is likely that attempts to compute the PV πNN couplings on the lattice will precede any efforts to study the short range PV interaction.

Historically, single nucleon, PV pion photo- and electroproduction processes were studied in the meson-exchange framework two decades ago by Woloshyn (119) and Li and Henley (120). These authors found that one should expect PV asymmetries for the scattering of longitudinally polarized photons to be of order a few $\times 10^{-7}$ assuming the DDH best value for h_π^1 , while those for electroproduction could be up to two orders of magnitude larger. Given the experimental challenges associated with such tiny asymmetries, and the prospect of measuring considerably larger effects in light nuclei, the prospects for carrying out single nucleon studies were largely ignored for many years.

Recently, however, advances in experimental techniques for measuring $\mathcal{O}(10^{-7})$ photo- and electroproduction asymmetries have stimulated renewed interest in this direction. Theoretically, Chen and Ji reformulated the earlier work for near threshold PV pion photo- (121) and electroproduction (122) using heavy baryon χ PT. Subleading contributions were subsequently considered by the authors of Reference (123). To $\mathcal{O}(Q)$, one has for the threshold photoproduction asymmetry

$$B_\gamma = \frac{\sqrt{2}F_\pi}{g_A m_N} \left[\mu_p - \mu_n \left(1 + \frac{m_\pi}{m_N} \right) \right] h_\pi^1 + \frac{4\sqrt{2}m_\pi \bar{C}_\pi}{g_A \Lambda_\chi} \quad (39)$$

where $\Lambda_\chi = 4\pi F_\pi$ and the terms proportional to m_π give the $\mathcal{O}(Q)$ contributions. A measurement at Jefferson Laboratory could in principle yield a result for B_γ with statistical accuracy at better than the 10^{-7} level; however, substantial technical challenges associated with the implied current mode pion detection would have to be overcome to design a successful experiment.

Considerably larger photo- and electroproduction asymmetries may be observed in the vicinity of the $\Delta(1232)$ resonance. The asymmetry in this region is dominated by

the lowest order PV $\gamma N \Delta$ interaction that does not contribute strongly at lower energies (124):

$$\mathcal{L}_{\text{PV}}^{\Delta N \gamma} = i \frac{e}{\Lambda_\chi} \left[d_\Delta^+ \bar{\Delta}_\mu^+ \gamma_\lambda p + d_\Delta^- \bar{\Delta}_\mu^0 \gamma_\lambda n \right] F^{\mu\lambda} + \text{h.c.} \quad (40)$$

where the d_Δ^\pm are low energy constants that govern the strength of the PV transition. For $E_\gamma \approx m_\Delta - m_N$, the PV photoproduction asymmetry is

$$B_\gamma^\pm \approx -\frac{2d_\Delta^\pm}{C_3^V} \frac{m_N}{\Lambda_\chi} + \dots \quad (41)$$

where $C_3^V \sim 2$ is the transition magnetic moment and where the “+...” indicate higher order, chiral corrections. The latter have been computed in Reference (125) and shown to be relatively small. Thus, the size of the resonance asymmetry is essentially set by d_Δ^\pm .

The authors of Reference (125) noted that a determination of d_Δ^\pm could provide additional insights into the puzzles surrounding the $\Delta S = 1$ HWI discussed earlier. In particular, if the dynamics responsible for the enhanced PV hyperon radiative decay asymmetries also occur for the $\Delta S = 0$ PV $N \rightarrow \Delta$ transition, then one might expect B_γ^\pm as large as a few $\times 10^{-6}$. Such an effect could be observed in forward angle PV electroproduction experiments, for which the contribution of Z^0 exchange becomes kinematically suppressed, thereby exposing the d_Δ contribution (125). On the other hand, if the occurrence of enhanced PV asymmetries is unique to the $\Delta S = 1$ sector and is associated with presence of valence strange quarks, then one would expect B_γ^\pm to smaller by an order of magnitude or more.

With this motivation in mind, possibilities for measuring B_γ^\pm using both the G0 and Q_{weak} instrumentation at Jefferson Lab are being actively pursued. The G0 collaboration will measure inclusive pion asymmetries in an upcoming backward angle run on a deuterium target (126). A measurement of the PV asymmetry in inclusive inelastic ep scattering at much lower Q^2 to $\simeq 0.09$ ppm is also envisioned as a future enhancement of the Q_{weak} experimental program (127).

As an alternative to photo- and electroproduction, one may also consider PV Compton scattering from the nucleon. Computations of the asymmetry for scattering with either polarized protons or polarized photons have been carried out in references (128) and (129). The asymmetry in both cases is proportional to h_π^1 at leading order. For $E_\gamma \ll m_\pi$ and center of mass scattering angle $\theta = \pi/2$ one has (129)

$$A_{\vec{\gamma}p \rightarrow \gamma p} \sim 8.8 \times 10^{-9} \left(\frac{h_\pi^1}{5 \times 10^{-7}} \right) \left(\frac{E_\gamma}{70 \text{ MeV}} \right)^3 \quad (42)$$

where one expects higher order corrections to yield corrections of order 25% and where h_π^1 has been scaled to the magnitude expected from NDA. Thus, one could expect to see an asymmetry of order a few $\times 10^{-8}$ – roughly the size of the asymmetry expected in $\vec{n} + p \rightarrow d + \gamma$. The magnitude of the asymmetry for Compton scattering with a polarized target is similar. To date, no experimental proposals have been developed for measuring either asymmetry.

Computing h_π^1 in QCD

Much of the recent theoretical focus has fallen on extracting the leading PV pion-nucleon coupling in a way that does not require knowledge of the other PV LEC's or of many-body nuclear physics. The interest in h_π^1 has also stimulated new analyses of QCD predictions for this quantity that attempt to go beyond the work of DDH. A first principles computation will ultimately require use of lattice QCD, and while we are not aware of immediate plans to carry out such a calculation, some of the necessary theoretical groundwork has been recently laid. In particular, tractable lattice computations typically involve use of quarks that are heavier than the physical light quarks, so in order to obtain a physically realistic QCD prediction from a lattice result, one needs to know the quark mass dependence of a given quantity¹¹. To that end, χ PT provides the necessary link, since the chiral expansion in powers of m_π is equivalent to an expansion in $\sqrt{m_q}$.

The first such analysis of h_π^1 was performed by the authors of Reference (130), who employed $SU(2)_L \times SU(2)_R$ χ PT with explicit Δ isobar degrees of freedom and computed all contributions to $\mathcal{O}(Q^3)$. These contributions arise from one-loop diagrams of the type illustrated in Figure 11. Naively, one expects the loop contributions to be suppressed by powers of $(Q/\Lambda_\chi)^k$ for $k = 2, 3$, where $\Lambda_\chi = 4\pi F_\pi \sim 1$ GeV and Q is either m_π or $m_\Delta - m_N$. In the case of h_π^1 , however, the one-loop contributions receive logarithmic and fortuitous numerical enhancements, leading to the renormalized coupling

$$h_\pi^1 = 0.5\mathring{h}_\pi^1 + 0.25h_A^1 - 0.24h_\Delta + 0.08h_A^\Delta \quad , \quad (43)$$

where \mathring{h}_π^1 is the bare πNN PV Yukawa coupling, h_Δ is the analogous PV $\pi N\Delta$ Yukawa coupling, h_A^1 parameterizes the isovector πNN PV derivative coupling

$$\mathcal{L}_A^{\pi NN} = i\frac{h_A^1}{F_\pi^2}\bar{N}\gamma^\mu\gamma_5N\left(\pi^+D_\mu\pi^- - \pi^-D_\mu\pi^+\right) + \dots \quad (44)$$

and h_A^Δ parameterizes analogous PV $\pi N\Delta$ derivative couplings.

The corrections appearing in Eq. (43) are only those having non-analytic quark mass dependence $m_q \ln m_q$ or $m_q^{3/2}$ (in the $m_\Delta = m_N$ limit) and are uniquely identified with chiral loops¹². As discussed in Reference (130), terms of this form cannot arise in quark model matrix elements of the hadronic weak Hamiltonian that were used in the analysis of DDH. Moreover, the ‘‘sum rule’’ contribution to h_π^1 that DDH derived from $\Delta S = 1$ decays using $SU(6)_w$ symmetry relied on tree-level symmetry relations that do not contain m_q -dependent symmetry breaking effects generated by chiral loops. Thus, it appears unlikely that DDH benchmark estimates for h_π^1 fully reflect the impact of its quark mass dependence. Interestingly, the magnitudes of the coefficients of the various terms in Eq. (43) are comparable, allowing for possible cancellations between them that could reduce the magnitude of h_π^1 from the DDH ‘‘best value’’. In principle, a study of h_π^1 on the lattice could allow one to identify the unknown constants appearing in Eq. (43) by varying both m_q and the number of colors.

At present, carrying out such an analysis with unquenched QCD is prohibitively expensive. An alternative approach that allows one to extrapolate lattice computations

¹¹The advent of chiral quarks has reduced the range over which an extrapolation must be performed.

¹²Terms that are analytic in m_q can be absorbed into corresponding terms in the Lagrangian

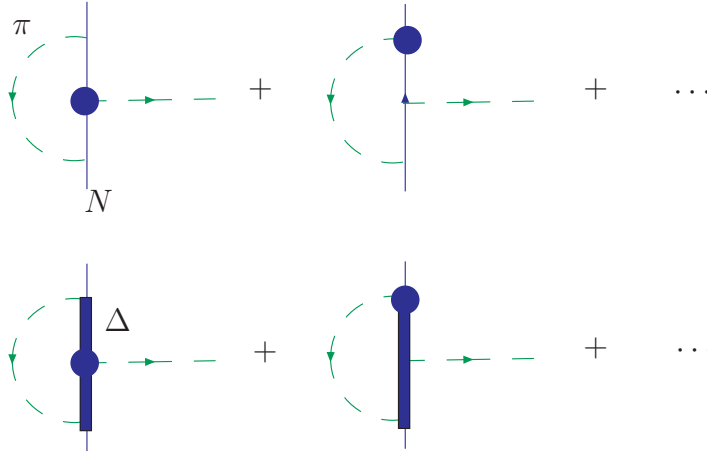


Figure 11: *One loop contributions to renormalized, PV πNN Yukawa coupling.*

to the domain of the physical, light quarks is to vary the valence and sea quark masses independently – a technique known as partial quenching. In order to identify the m_q^{valence} and m_q^{sea} dependence analytically from one-loop computations, one must generalize standard χ PT to the corresponding partially-quenched effective theory (131). A computation using this framework has been performed in Reference (132), leading to an analogous expression to that of Eq. (43) that gives the non-analytic valence and sea quark mass dependence in the partially-quenched theory. An extrapolation to the chiral domain also requires inclusion of analytic terms that can be obtained from the effective Lagrangian and that were not written down explicitly in Reference (132).

As of this writing, the first-principles QCD analysis of h_π^1 has not advanced beyond the analytic work of references (130, 132). Given the new experimental efforts, the time is clearly right for an investment in a lattice computation of h_π^1 . On a longer term horizon, one would also hope to see lattice predictions of the constants C_i and \tilde{C}_i that parameterize the $\mathcal{O}(Q)$ short-distance, PV four-nucleon operators discussed above. Obtaining such computations will likely depend on progress in lattice calculations of the low-energy, strong NN interaction. A program aimed in this direction is being carried out by Savage and collaborators (M.J. Savage, private communication).

In the absence of first principles QCD computations of the PV constants, one may look to nucleon model calculations for guidance as to their magnitudes. The expectations derived from the DDH $SU(6)_w$ /quark model treatment (6) has been discussed above. Alternate approaches have recently been used to predict h_π^1 . In the three-flavor Skyrme model of Reference (133), the dominant contribution arises from terms in the $\Delta S = 0$, PV four-quark Hamiltonian that contain strange quark bilinears such as $\bar{s}\gamma^\mu s \bar{u}\gamma_\mu \gamma_5 u$. These terms sample the “kaon cloud” that arises from the Wess-Zumino action via rotations of the chiral soliton in $SU(3)$ space. The resulting prediction is $2g_\pi \lesssim h_\pi^1 \lesssim 3.4g_\pi$. The corresponding prediction in the two-flavor Skyrme model is considerably smaller. A prediction for a somewhat larger value has been obtained using QCD sum rules (134),

wherein one expands nucleon correlators in a pion background in terms of various quark and gluon condensates. Values for the latter – such as $\langle \bar{q}i\tau^a\gamma_5q \rangle_\pi$ – are taken from other nucleon properties, such as the strong πNN coupling, leading to $h_\pi^1 \sim 8g_\pi$. Both sets of model predictions are roughly consistent with expectations based on NDA as well as the updated “best values” obtained from the $SU(6)_w$ /quark model approach (6, 12)

3.4 Experimental Prospects

In the foregoing sections, we have emphasized the need for a complete set of precise PV measurements in the NN and few nucleon systems that can be cleanly interpreted in terms of constraints on PV LECs. As summarized in Table 3, we have currently two significant measurements in hand carried out with low energy proton beams (A_z^{pp} and $A_z^{p\alpha}$), and two currently underway at existing neutron facilities (A_γ^d and $d\phi^{n\alpha}/dz$). As noted earlier, there is also an existing pd asymmetry measurement (99) which poses additional theoretical challenges accounting for the angular dependence in both elastic scattering and breakup channels, that remains to be analyzed in a common framework.

Some immediate prospects for improvement in neutron beam measurements will take advantage of the superior features of a high intensity pulsed beam facility, the Spallation Neutron Source (SNS), currently under construction at Oak Ridge, Tennessee. The SNS is anticipated to provide the world’s most intense beams of cold pulsed neutrons, approaching or even surpassing the time averaged intensities of cw reactor sources (135) by 2008. A crucial advantage of pulsed beams over reactor sources for precision PV experiments results from the introduction of new diagnostic capabilities via time-of-flight analysis of the neutron energy – especially important for reducing γ -ray backgrounds and systematic error diagnosis as well as neutron polarization diagnostics. In addition, the construction of a new facility allows for the incorporation of technological advances in neutron guide instrumentation, particularly the use of high efficiency bent supermirror transport guides which eliminate direct line of sight between the apparatus and the cold moderator, thereby reducing γ -ray and neutron backgrounds without significant loss of beam flux. The SNS is building a new dedicated beamline for Fundamental Neutron Physics (FnPB) (135, 136) which is optimized to the needs of a suite of precision experiments in HWI and neutron beta decay.

Neutron Capture Gamma Asymmetry Measurements

As discussed earlier, the LANSCE phase of the ongoing NPDGamma experiment to measure A_γ^d will be statistics limited at the 10^{-7} level, while the expected asymmetry based on the NDA and DDH ‘best value’ estimates for h_π^1 is $A_\gamma^d = -5 \times 10^{-8}$. NPDGamma is expected to be a key element of the initial SNS fundamental neutron physics program (137). At the time of writing, the apparatus has been commissioned, and systematic errors have been extensively studied at LANSCE, awaiting installation of the liquid parahydrogen target. A conclusion of these studies is that the apparatus is ready to make a measurement of A_γ^d with a statistical error of 1×10^{-8} . Systematic errors are expected to be at or below the 10^{-9} level; however, additional running time to measure the potential false asymmetry from aluminum vacuum windows is needed to reach the ultimate experimental precision that can be achieved at the SNS.

The SNS FnpB beamline has been extensively studied via Monte Carlo simulations, and reasonably conservative flux estimates indicate that a measurement of A_γ^d at the 1×10^{-8} level should be possible in approximately 5000 hours of running on the new beamline once the SNS reaches 1.4 MW operation. The experiment can be moved with only minimal changes required to the apparatus, since the beam conditions (apart from increased flux) will be quite similar to those at LANSCE. It is planned to use the NPDGamma apparatus to commission the new FnpB beamline when it comes on line, beginning in 2008. In addition to the higher beam flux, two significant improvements in experimental conditions at the SNS are anticipated that could further improve the experimental precision. Gamma background reduction will be achieved in part as a result of the SNS curved neutron guide, and in part with the incorporation of additional lead shielding upstream of the main detector array. Higher beam polarization should also be possible, via a combination of increased laser pumping power and/or the use of spectrally narrowed lasers for optical pumping of the ^3He spin filter cell, which have been demonstrated to produce up to 75% polarization in bench tests as compared to 40-55% ^3He polarization routinely achieved during extended running in FP12 at LANSCE (137).

As noted earlier, the PV gamma asymmetry A_γ^t in the reaction $\vec{n} + d \rightarrow t + \gamma$ provides a complementary window on the $\Delta S = 0$ HWI to its counterpart in the np system. A Letter of Intent has been submitted to the SNS to develop this experiment as a logical follow up to the NPDGamma experiment (138). As indicated in Table 3, A_γ^t displays a much larger sensitivity to the PV LEC's – including a ~ 30 times stronger sensitivity to h_π^1 – than does A_γ^d . Based on the various estimates for the PV LECs (Table 2), one could expect A_γ^t to be one to two orders of magnitude larger than A_γ^d .

In principle, the nd asymmetry measurement can be performed using most of the components of the NPDGamma apparatus, with an obvious exception of the target. The experiment is technically much more challenging than the np case due to the much smaller nd capture cross section; consequently, most of the neutrons will scatter out of the target rather than being captured to produce the gamma rays of interest. A room temperature liquid D_2O target is under consideration, with a length optimized between two competing factors – the very small nd capture cross section, and the desire to avoid significant neutron depolarization in the target. A novel target vessel and shielding scheme will be required to absorb the scattered neutrons without producing significant background gamma rays. The interactions of polarized cold neutrons in D_2O are at present not well understood, and a program of detailed simulations and test measurements will be carried out in order to optimize the design of the experiment. Other target possibilities include cold solid orthodeuterium or solid ortho- D_2O in an effort to minimize depolarization by slowing down the neutron beam, thereby increasing the capture probability (W. M. Snow, private communication). An earlier measurement of A_γ^t was carried out at ILL and found a result consistent with zero: $A_\gamma^t = (4.2 \pm 3.8) \times 10^{-6}$ (139, 140); the goal of the proposed SNS measurement is to reach a sensitivity 4×10^{-7} . Many of the systematic effects are similar to those for the np experiment, where they have been extensively studied. It should be noted that the absolute tolerance for systematic errors is relaxed for the nd experiment, since the absolute precision goal is more than an order of magnitude less stringent than that for the np experiment.

Neutron Spin Rotation Measurements

As for the neutron capture asymmetry measurements, the higher neutron flux anticipated for the SNS as well as the pulsed nature of the beam offer compelling advantages for improving the precision of the $n\alpha$ PV spin rotation measurement, as well as the possibility of carrying out experiments on np and perhaps even nd spin rotation. To date, a Letter of Intent has been submitted for the $n\alpha$ experiment (141), anticipating a measurement accuracy of 1×10^{-7} rad/m in 12 months of data taking, which would represent a factor of three improvement over what is currently expected at NIST, with improved systematic error control. It is likely that the $n\alpha$ spin rotation experiment will run at the SNS quite early in the FnPB experimental program. The collaboration intends in the longer term to pursue np spin rotation at the SNS as well (142). The sensitivity of the $n\alpha$ spin rotation experiment to the five PV LEC's in the pionless EFT is given in table 3 (predictions in the DDH meson-exchange model are available for the np and $n\alpha$ cases, as mentioned in Section 2.2.3).

The basic spin rotation experimental technique has been outlined in Section 2.2.3; recall the crucial role of the ‘ π coil’ in Figure 10, which is used to suppress the effect of the much larger spin precessions due to residual magnetic fields inside the apparatus. Since previous experiments have been carried out at reactor facilities with polychromatic cold neutron beams, the best one could do was to optimize the field in the π coil to rotate the neutron spins on average by 180° between the upstream and downstream segments of the apparatus. Nearly a factor of two improvement can be obtained at a pulsed source (142) by ramping the π coil current as a function of time of flight to provide a 180° spin rotation for all neutron velocities. In addition, one can take advantage of the fact that the PV spin rotation is independent of neutron velocity, whereas scattering and magnetic field effects are in general energy and thus velocity dependent for diagnosis of systematic effects. For the hydrogen and possible deuterium target measurements, neutron depolarization must be avoided by preparing cryogenic liquid targets in spin-selected molecular states - paramolecular for hydrogen and orthomolecular for deuterium - an additional complication, particularly considering the requirement for constant cycling of the liquid between “front” and “rear” target locations. For neutron energies below 15 meV, depolarization does not occur in parahydrogen. Less is known about the case for orthodeuterium, but a recent measurement at PSI found negligible depolarization of cold neutrons on orthodeuterium for a 4 cm target (W. M. Snow, private communication), which is encouraging news for the prospect of a deuterium spin rotation measurement.

4 Beyond Hadronic Parity Violation

Throughout this article, we have emphasized the significance of hadronic PV as a probe of the strangeness conserving HWI. Here, we comment briefly on its implications for other processes. We have already encountered one such process – PV electron scattering – discussed in Section 2.1. There, contributions from hadronic PV to the PV asymmetries constitutes a theoretical background that one must compute reliably in order to extract information on other quantities of interest, such as the strange quark form factors.

A second illustration concerns neutrinoless double β -decay ($0\nu\beta\beta$). This process has

considerable current interest, as it provides the only known way to determine whether or not neutrinos are Majorana fermions (for recent reviews, see *e.g.*, references (143, 144).) In addition, one also hopes to use $0\nu\beta\beta$ to determine the absolute scale of neutrino mass, complementing what we know about m_ν from tritium β -decay and about neutrino mass differences from oscillation studies.

Unfortunately, the latter use of $0\nu\beta\beta$ is complicated by possible contributions to the rate from the exchange of heavy Majorana particles, such as a heavy Majorana neutrino or the neutralinos of supersymmetry. In order to determine the absolute scale of m_ν , one must know the amplitude A_H for heavy particle-exchange contributions, which can be comparable in magnitude to the amplitude A_L for light Majorana neutrino-exchange. From simple dimensional arguments, one has (145)

$$\frac{A_H}{A_L} \sim \frac{M_W^4 \bar{k}^2}{\Lambda^5 m_{\beta\beta}} \quad , \quad (45)$$

where $m_{\beta\beta}$ is the effective mass of the light Majorana neutrino having typical virtuality $\bar{k}^2 \sim (50 \text{ MeV})^2$ and Λ is the mass scale associated with the heavy Majorana particles. Given what we know about Δm_ν^2 and the neutrino mixing matrix elements that help determine $m_{\beta\beta}$, the ratio in Eq. (45) can be $\mathcal{O}(1)$ for Λ of order 1 TeV. Thus, it is important to analyze the possible heavy particle contributions with theoretical clarity.

Recently, an EFT approach for doing so was developed by the authors of Reference (146). At the lepton-quark level, the effective operators for heavy, Majorana particle exchange factorize into products of four-quark and two-lepton operators. The four-quark operators are analogous to those entering the $\Delta S = 0$ HWI, differing only in their respective representations in chiral SU(2). Consequently, the mapping of these operators onto effective, hadronic operators involving nucleon and pion degrees of freedom is similar to the one used in obtaining the EFT for hadronic PV. Thus, the study of hadronic PV should provide insights into the EFT for heavy particle contributions in $0\nu\beta\beta$. We consider two aspects of this correspondence in particular:

- (i) In contrast to the situation for hadronic PV, there does not exist a program of few-body experiments from which one can determine the operator coefficients for the $0\nu\beta\beta$ EFT. These coefficients must be computed theoretically. Comparisons of analogous computations of the LECs for hadronic PV with experimental values should provide new guidance for obtaining reliable computations in the $0\nu\beta\beta$ case. Indeed, as argued above, hadronic PV provides a unique tool for learning how the strong interaction dresses four-quark weak interactions into hadronic operators and amplitudes.
- (ii) Again in contrast to hadronic PV, the only systems in which $0\nu\beta\beta$ can occur are heavy, complex nuclei. While there has been considerable recent progress in understanding how an EFT power-counting of operators translates into a power-counting of few-body matrix elements, the situation with complex nuclei is less clear. In order for the EFT to provide realistic guidance to the size of heavy particle contributions to $0\nu\beta\beta$ transition matrix elements, we need to know how well operator power counting works for nuclear matrix elements.

In principle, hadronic PV can provide useful insights into this issue. Since the lowest order PV interaction can be determined from a program of few-body experiments as outlined above, this interaction can then be used as a known probe of nuclear PV observables, such as the nuclear anapole moment or the PV γ -decays of p-shell nuclei. To the extent that the lowest order PV interaction suffices to yield successful descriptions of these nuclear PV observables, we would have evidence for the applicability of the EFT to nuclei. To the extent that it does not, we would conclude that many-body renormalization of the lowest-order weak effective interaction is substantial and that high-momentum components of nuclear wave-functions play a more important role than one might naively expect. Either way, the implications for $0\nu\beta\beta$ would be important.

5 Summary and Conclusions

The quest to explain the manifestations of weak interactions between quarks in strongly-interacting systems remains an important piece of “unfinished business” for Standard Model physics. In both the $\Delta S = 1$ and $\Delta S = 0$ sectors, the non-perturbative character of low-energy QCD has been the stumbling block. The $\Delta S = 1$ decays of hyperons in particular seem to elude explanation using the standard symmetry and effective field theory approaches that have been so successful in treating low-energy strong interactions. Whether these puzzles simply reflect the active participation of the strange quark with its mass of order the QCD scale, or some other dynamics peculiar to hadronic weak interactions, is unknown. Our hope is that through experimental studies of the $\Delta S = 0$ HWI with PV observables and through their theoretical interpretation within the EFT framework that makes for the closest possible contact with QCD, we will gain new insights into the low-energy weak interactions of the three lightest quarks. In this review, we hope to have sketched a useful roadmap for future progress in this direction.

As we have emphasized throughout this article, the forefront in this endeavor lies in the arena of single-nucleon and few-body nuclear systems. Experimental developments have paved the way for completion of precise measurements of the $\mathcal{O}(10^{-7})$ PV effects in such systems, and plans are underway for several new few-body experiments. The immediate theoretical challenge is to compute the few-body PV observables using the EFT framework, allowing one to extract robust values for the low energy constants from experiment. In the longer term, we would like to determine the extent to which these results are consistent with Standard Model-based expectations, both from the standpoint of symmetries and from first principles lattice calculations. In light of the substantial experimental and theoretical progress in the field as well as the significant new opportunities made possible by this progress, we are optimistic that this effort can be successful.

6 Acknowledgements

The authors would like to thank J. Carlson, B. Desplanques, M. T. Gericke, G. Gwinner, G. L. Greene, W.C. Haxton, B. R. Holstein, C.-P. Liu, C. Maekawa, W. M. Snow, U. van Kolck and S.-L. Zhu, for helpful discussions. This work was supported in part under DOE contract FG02-05ER41361, NSF Award PHY-0071856, and by grants from NSERC (Canada) and the NSF.

LITERATURE CITED

1. Tanner N. 1957. *Phys. Rev.* 107 1203
2. Feynman R, Gell-Mann M. 1958. *Phys. Rev.* 109 193
3. Lobashov VM, et al. 1967. *Sov. Phys. JETP* 5 59
4. Lobashov VM, et al. 1967. *Phys. Lett. B* 25 104
5. Bowman CD, Bowman JD, Yuan VW. 1989. *Phys. Rev.* C39 1721–1724
6. Desplanques B, Donoghue JF, Holstein BR. 1980. *Ann. Phys.* 124 449
7. Haxton WC, Liu CP, Ramsey-Musolf MJ. 2002. *Phys. Rev.* C65 045502
nucl-th/0109014
8. Zhu SL, et al. 2005. *Nucl. Phys.* A748 435–498 nucl-th/0407087
9. Adelberger EG, Haxton WC. 1985. *Ann. Rev. Nucl. Part. Sci.* 35 501–558
10. Desplanques B. 1998. *Phys. Rept.* 297 1–61
11. Dubovik VM, Zenkin SV. 1986. *Annals Phys.* 172 100–135
12. Feldman GB, Crawford GA, Dubach J, Holstein BR. 1991. *Phys. Rev.* C43 863–874
13. Barton G. 1961. *Nuovo Cim.* 19 512–527
14. Holstein BR. 1981. *Phys. Rev.* D23 1618–1623
15. Holstein BR. 2004. *Nucl. Phys.* A737 85–92
16. Zeldovich Y. 1958. *Sov. Phys. JETP* 6 1184
17. Musolf MJ, Holstein BR. 1991. *Phys. Rev.* D43 2956–2970
18. Flambaum VV, Khriplovich IB. 1980. *Sov. Phys. JETP* 52 835
19. Flambaum VV, Khriplovich IB, Sushkov OP. 1984. *Sov. Phys. JETP* 60 873
20. Haxton WC, Wieman CE. 2001. *Ann. Rev. Nucl. Part. Sci.* 51 261–293
nucl-th/0104026

21. Dmitriev VF, Khriplovich IB. 2004. *Phys. Rept.* 391 243–260 [nucl-th/0309083](#)
22. Ginges JSM, Flambaum VV. 2004. *Phys. Rept.* 397 63–154 [physics/0309054](#)
23. Haxton WC, Henley EM, Musolf MJ. 1989. *Phys. Rev. Lett.* 63 949
24. Haxton WC, Liu CP, Ramsey-Musolf MJ. 2001. *Phys. Rev. Lett.* 86 5247–5250
[nucl-th/0101018](#)
25. Bouchiat C, Piketty CA. 1991. *Z. Phys.* C49 91–108
26. Bouchiat C, Piketty CA. 1991. *Phys. Lett.* B269 195–200
27. Dmitriev VF, Khriplovich IB, Telitsin VB. 1994. *Nucl. Phys.* A577 691–708
[nucl-th/9401021](#)
28. Dmitriev VF, Telitsin VB. 2000. *Nucl. Phys.* A674 168–184 [nucl-th/9912004](#)
29. Wilburn WS, Bowman JD. 1998. *Phys. Rev.* C57 3425–3429 [nucl-ex/9802006](#)
30. Auerbach N, Brown BA. 1999 [nucl-th/9903032](#)
31. Bennett LM C, Krien K. 1980. *Bull. Am. Phys. Soc.* 25 486
32. Haxton WC. 1981. *Phys. Rev. Lett.* 46 698
33. Musolf MJ, Holstein BR. 1990. *Phys. Lett.* B242 461–466
34. Musolf MJ, Donnelly TW. 1992. *Nucl. Phys.* A546 509–587
35. Musolf MJ, et al. 1994. *Phys. Rept.* 239 1–178
36. Hasty R, et al. (SAMPLE). 2000. *Science* 290 2117 [nucl-ex/0102001](#)
37. Zhu SL, Puglia SJ, Holstein BR, Ramsey-Musolf MJ. 2000. *Phys. Rev.* D62 033008
[hep-ph/0002252](#)
38. Riska DO. 2000. *Nucl. Phys.* A678 79–109 [hep-ph/0003132](#)
39. Maekawa CM, van Kolck U. 2000. *Phys. Lett.* B478 73–78 [hep-ph/0006161](#)
40. Maekawa CM, Veiga JS, van Kolck U. 2000. *Phys. Lett.* B488 167–174
[hep-ph/0006181](#)
41. Schiavilla R, Carlson J, Paris MW. 2003. *Phys. Rev.* C67 032501 [nucl-th/0212038](#)
42. Liu CP, Prezeau G, Ramsey-Musolf MJ. 2003. *Phys. Rev.* C67 035501
[nucl-th/0212041](#)
43. Ito TM, et al. (SAMPLE). 2004. *Phys. Rev. Lett.* 92 102003 [nucl-ex/0310001](#)
44. Spayde DT, et al. (SAMPLE). 2004. *Phys. Lett.* B583 79–86 [nucl-ex/0312016](#)

45. Bowman JD, Garvey GT, Johnson MB, Mitchell GE. 1993. *Ann. Rev. Nucl. Part. Sci.* 43 829–881
46. Simonius M. 1988. *Can. J. Phys.* 66 548–553
47. Berdoz AR, et al. (TRIUMF E497). 2003. *Phys. Rev.* C68 034004 [nucl-ex/0211020](#)
48. Levy C, et al. 1994. *AIP Conf. Proc.* 293 179
49. Zelenski AN, et al. 1993. *Nucl. Instrum. Meth.* A334 285–293
50. Berdoz AR, et al. 2001. *Nucl. Instrum. Meth.* A457 288–298 [physics/0011007](#)
51. Ramsay W, et al. 2002. *Proc. 9th Intl. Workshop on Pol. Sources and Targets (World Scientific)* 289
52. Eversheim PD, et al. 1991. *Phys. Lett.* B256 11–14
53. Kistryn S, et al. 1987. *Phys. Rev. Lett.* 58 1616
54. Carlson J, Schiavilla R, Brown VR, Gibson BF. 2002. *Phys. Rev.* C65 035502 [nucl-th/0109084](#)
55. Driscoll DE, Miller GA. 1989. *Phys. Rev.* C40 2159–2167
56. Driscoll DE, Miller GA. 1989. *Phys. Rev.* C39 1951–1962
57. Iqbal MJ, Niskanen JA. 1994. *Phys. Rev.* C49 355–359
58. Driscoll DE, Meissner UG. 1990. *Phys. Rev.* C41 1303–1305
59. Grach I, Shmatikov M. 1993. *Phys. Lett.* B316 467–471
60. Wiringa RB, Stoks VGJ, Schiavilla R. 1995. *Phys. Rev.* C51 38–51 [nucl-th/9408016](#)
61. Machleidt R. 2001. *Phys. Rev.* C63 024001 [nucl-th/0006014](#)
62. Fujiwara M, Titov AI. 2004. *Phys. Rev.* C69 065503 [nucl-th/0403004](#)
63. Knyazkov V, et al. 1984. *Nucl. Phys.* A 417 209
64. Earle ED, et al. 1988. *Can. J. Phys.* 66 534–541
65. Cavaignac JF, Vignon B, Wilson R. 1977. *Phys. Lett.* B67 148–150
66. Oka T. 1983. *Phys. Rev.* D27 523–530
67. Schiavilla R, Carlson J, Paris MW. 2004. *Phys. Rev.* C70 044007 [nucl-th/0404082](#)
68. Khriplovich IB, Korkin RV. 2001. *Nucl. Phys.* A690 610–620 [nucl-th/0005054](#)
69. Liu CP, Hyun CH, Desplanques B. 2004. *Phys. Rev.* C69 065502 [nucl-th/0403009](#)

70. Stiliaris E. 2005. *Eur. Phys. J.* 24 S2 175
71. Carlson J, Paris M. 2005. *Eur. Phys. J.* A24S1 123–125
72. Gericke MT, et al. (NPDGamma). 2005 nucl-ex/0507005
73. Gericke MT, et al. 2005. *Nucl. Instrum. Meth.* A540 328–347 nucl-ex/0411022
74. Stodolsky L. 1982. *Nucl. Phys.* B197 213
75. Bass C, et al. 2005. *J. Res. Nat. Inst. Stand. Technol.* 110 205–208
76. Markoff D. 1997. *Measurement of the Parity Nonconserving Spin-Rotation of Transmitted Cold Neutrons Through a Liquid Helium Target* Ph.D. thesis University of Washington
77. Dmitriev FVVSOP V, Telitsin VB. 1983. *Phys. Lett.* 125 125
78. Bass C, et al. 2005. *unpublished*
79. Wood CS, et al. 1997. *Science* 275 1759–1763
80. Vetter PA, et al. 1995. *Phys. Rev. Lett.* 74 2658–2661
81. Guera J, et al. 2005. *Phys. Rev. A* 71 042108
82. Dzuba VA, Flambaum VV, Khriplovich IB. 1986. *Z. Phys.* D 1 243
83. DeMille D. 1995. *Phys. Rev. Lett.* 74 4165
84. Stalnaker J, et al. 2002. *Phys. Rev. A* 66 031403(R)
85. Gomez ASOLASGD E, DeMille D. 2004. *arXiv:physics* 0412124
86. Koerber T, et al. 2003. *J. Phys B* 36 637
87. Gomez E, et al. 2006. *Rep. Prog. Phys.* 69 79
88. Grossman JS, et al. 1999. *Phys. Rev. Lett.* 83 935
89. Gwinner G, et al. 2005. *TRIUMF EEC Proposal* E 1065
90. Mitchell BJPS GE, Sharapov E. 2001. *Phys. Rep.* 354 157
91. Tomsovic S, Johnson MB, Hayes A, Bowman JD. 2000. *Phys. Rev.* C62 054607 nucl-th/9911057
92. Danilov G. 1965. *Phys. Lett.* 18 40
93. Desplanques B, Missimer J. 1978. *Nucl. Phys.* A300 286–312
94. Desplanques B, Benayoun JJ. 1986. *Nucl. Phys.* A458 689–708

95. Miller GA. 2003. *Phys. Rev.* C67 042501 nucl-th/0301012
96. Lang J, et al. 1985. *Phys. Rev. Lett.* 54 170–173
97. Alberi J, et al. 1988. *Can. J. Phys.* 66 542–547
98. Kloet WM, Gibson BF, Stephenson GJ, Henley EM. 1983. *Phys. Rev.* C27 2529–2544
99. Kistryn S, et al. 1989. *Phys. Lett.* B219 58–61
100. Fleming S, Mehen T, Stewart IW. 2000. *Nucl. Phys.* A677 313–366 nucl-th/9911001
101. Kaplan DB, Savage MJ, Wise MB. 1998. *Phys. Lett.* B424 390–396 nucl-th/9801034
102. Kaplan DB, Savage MJ, Wise MB. 1998. *Nucl. Phys.* B534 329–355 nucl-th/9802075
103. Weinberg S. 1990. *Phys. Lett.* B251 288–292
104. Weinberg S. 1991. *Nucl. Phys.* B363 3–18
105. Beane SR, Bedaque PF, Savage MJ, van Kolck U. 2002. *Nucl. Phys.* A700 377–402 nucl-th/0104030
106. Beane SR, Savage MJ. 2003. *Nucl. Phys.* A713 148–164 hep-ph/0206113
107. Beane SR, Savage MJ. 2003. *Nucl. Phys.* A717 91–103 nucl-th/0208021
108. Kaplan DB, Savage MJ. 1993. *Nucl. Phys.* A556 653–671
109. Pirner HJ, Riska DO. 1973. *Phys. Lett.* B44 151–154
110. Manohar A, Georgi H. 1984. *Nucl. Phys.* B234 189
111. Kaplan DB, Savage MJ, Springer RP, Wise MB. 1999. *Phys. Lett.* B449 1–5 nucl-th/9807081
112. Desplanques B. 2001. *Phys. Lett.* B512 305–313 nucl-th/0006065
113. Savage MJ. 2001. *Nucl. Phys.* A695 365–373 nucl-th/0012043
114. Hyun CH, Park TS, Min DP. 2001. *Phys. Lett.* B516 321–326 nucl-th/0101043
115. Savage MJ, Springer RP. 1998. *Nucl. Phys.* A644 235–244 nucl-th/9807014
116. Savage MJ, Springer RP. 2001. *Nucl. Phys.* A686 413–428 nucl-th/9907069
117. Hyun CH, Desplanques B. 2003. *Phys. Lett.* B552 41–47 nucl-th/0206017

118. Liu CP, Hyun CH, Desplanques B. 2003. *Phys. Rev.* C68 045501 nucl-th/0306020
119. Woloshyn RM. 1979. *Can. J. Phys.* 57 809
120. Li SP, Henley EM, Hwang WYP. 1982. *Annals Phys.* 143 372–412
121. Chen JW, Ji XD. 2001. *Phys. Rev. Lett.* 86 4239–4242 hep-ph/0011230
122. Chen JW, Ji XD. 2001. *Phys. Lett.* B501 209–215 nucl-th/0011100
123. Zhu SL, Puglia S, Holstein BR, Ramsey-Musolf MJ. 2001. *Phys. Rev.* C64 035502 hep-ph/0012253
124. Zhu SL, Maekawa CM, Holstein BR, Ramsey-Musolf MJ. 2001. *Phys. Rev. Lett.* 87 201802 hep-ph/0106216
125. Zhu SL, et al. 2002. *Phys. Rev.* D65 033001 hep-ph/0107076
126. Martin J. 2003. *Eur. Phys. J. A* 18 425
127. Forest TA, et al. 2003. *JLab Letter of Intent* LOI-03-105
128. Bedaque PF, Savage MJ. 2000. *Phys. Rev.* C62 018501 nucl-th/9909055
129. Chen JW, Cohen TD, Kao CW. 2001. *Phys. Rev.* C64 055206 nucl-th/0009031
130. Zhu SL, Puglia SJ, Holstein BR, Ramsey-Musolf MJ. 2001. *Phys. Rev.* D63 033006 hep-ph/0005281
131. Sharpe SR, Shoresh N. 2000. *Phys. Rev.* D62 094503 hep-lat/0006017
132. Beane SR, Savage MJ. 2002. *Nucl. Phys.* B636 291–304 hep-lat/0203028
133. Meissner UG, Weigel H. 1999. *Phys. Lett.* B447 1–7 nucl-th/9807038
134. Henley EM, Hwang WYP, Kisslinger LS. 1996. *Phys. Lett.* B367 21–27 nucl-th/9511002
135. Greene GL, et al. 2005. *J. Res. Nat. Inst. Stand. Technol.* 110 149
136. Huffman P, et al. 2005. *J. Res. Nat. Inst. Stand. Technol.* 110 161
137. Bowman J, et al. 2005. *SNS - FNPB Letter of Intent*
138. Penttila S, et al. 2005. *SNS - FNPB Letter of Intent*
139. Avenier M, et al. 1986. *Nucl. Phys.* A 459 335
140. Alberi J, et al. 1988. *Can. J. Phys.* 66 542–547
141. Bass C, et al. 2005. *SNS - FNPB Letter of Intent* unpublished
142. Markoff DM. 2005. *J. Res. Nat. Inst. Stand. Technol.* 110 209

143. McKeown RD, Vogel P. 2004. *Phys. Rept.* 394 315–356 hep-ph/0402025
144. Elliott SR, Engel J. 2004. *J. Phys.* G30 R183 hep-ph/0405078
145. Cirigliano V, Kurylov A, Ramsey-Musolf MJ, Vogel P. 2004. *Phys. Rev. Lett.* 93 231802 hep-ph/0406199
146. Prezeau G, Ramsey-Musolf M, Vogel P. 2003. *Phys. Rev.* D68 034016 hep-ph/0303205